

Non-Hermitian Topological Mott Insulators in 1D Fermionic Superlattices

Tao Liu,^{1,*} James Jun He,² Tsuneya Yoshida,^{3,4} Ze-Liang Xiang,⁵ and Franco Nori^{1,6,†}

¹Theoretical Quantum Physics Laboratory, RIKEN Cluster for Pioneering Research, Wako-shi, Saitama 351-0198, Japan

²RIKEN Center for Emergent Matter Science, Wako, Saitama 351-0198, Japan

³Graduate School of Pure and Applied Sciences, University of Tsukuba, Tsukuba, Ibaraki, 305-8571, Japan.

⁴Department of Physics, University of Tsukuba, Tsukuba, Ibaraki, 305-8571, Japan.

⁵School of Physics, Sun Yat-sen University, Guangzhou 510275, China

⁶Department of Physics, University of Michigan, Ann Arbor, Michigan 48109-1040, USA

(Dated: July 19, 2022)

We study interaction-induced Mott insulators, and their topological properties in a 1D non-Hermitian strongly-correlated spinful fermionic superlattice system in the presence of nonreciprocal hopping. Our results show that the low-energy neutral excitation spectrum is sensitive to boundary conditions, which is a manifestation of the non-Hermitian skin effect. Moreover, the anomalous boundary effect occurs due to the interplay of nonreciprocal hopping, superlattice potential, and strong correlations, where some in-gap modes, for both the neutral and charge excitation spectra, show no edge excitations defined via only the right eigenvectors. We show that these edge excitations of the in-gap states can be correctly characterized by only biorthogonal eigenvectors. Our studies pave new routes towards exploring exotic topological features in non-Hermitian systems.

Introduction.—Recent years have witnessed considerable interest in exploring topological phases of non-Hermitian systems [1–59], which can be realized in classical optical and mechanical systems with gain and loss [60–75], correlated and disordered electronic systems with finite quasiparticle lifetimes [76–80], and open quantum systems with post-selection measurements [81]. Non-Hermitian topological systems exhibit many unique properties with no counterpart in Hermitian cases, such as: non-Hermitian skin effect and breakdown of the conventional bulk-boundary correspondence [17–19], bulk Fermi arcs [12], and rich Bernard-LeClair symmetry classes beyond the ten-fold Altland-Zirnbauer ones [24–26]. However, most of these studies have focused on non-Hermitian topological band theories at the single-particle level, and only very few recent works [59, 82] have studied strongly correlated non-Hermitian topological phases.

Rather than destroy the topological properties, the strong correlation can give rise to novel topological phases for Hermitian systems [83–92]. For example, interactions lead to fractional Chern insulators with exotic fractional quasiparticles obeying fractional statistics [83–86]. In addition, interactions result in topological Mott insulators [88, 89]: interactions open a nontrivial gap in the bulk, inducing single-particle gapless excitations around the boundary [93]. Up to now, studies of strongly correlated topological phases have been largely restricted to Hermitian systems. It is important to explore how topology and interactions interplay with non-Hermitian effects, leading to novel topological features without its Hermitian counterpart. In particular, in the single-particle case, nonreciprocal hopping causes the localization of eigenstates to the boundaries. This non-Hermitian skin effect, which leads to the breakdown of the bulk-boundary correspondence, does not cause the same localization in a fermionic many-body system [57].

This leads us to ask: Does nonreciprocal hopping lead to anomalous boundary effects in a non-Hermitian strongly correlated topological system?

In this paper, we address this important question by studying a non-Hermitian strongly correlated system in a 1D spin-1/2 fermionic superlattice system in the presence of nonreciprocal hopping. Our results show that interactions can drive the trivial non-Hermitian system into a topological Mott phase, and there exist both gapless neutral and charge excitations localized at the edges. Due to nonreciprocal hopping, the low-energy neutral excitation spectrum is sensitive to the boundary conditions, where the in-gap states emerge in the open chain in spite of the absence of gap in the periodic chain. This shows the impact of the non-Hermitian skin effect. We also found that some in-gap states, for both neutral and charge excitation spectra, show no edge excitations defined via only the right eigenvectors. This anomalous boundary effect results from the interplay of nonreciprocal hopping, superlattice potential, and interactions. Furthermore, these edge excitations can be characterized by using biorthogonal eigenvectors.

Model.—We consider a 1D model of spin-1/2 ultracold fermionic atoms loaded in a bichromatic optical lattice (see Sec. II(E) in the Supplemental Material [94]), described by

$$\mathcal{H} = -t \sum_{j,\sigma} \left(e^{\alpha} c_{j+1,\sigma}^{\dagger} c_{j,\sigma} + e^{-\alpha} c_{j,\sigma}^{\dagger} c_{j+1,\sigma} \right) + \sum_{j,\sigma} V_j n_{j,\sigma} + U \sum_j c_{j,\uparrow}^{\dagger} c_{j,\downarrow}^{\dagger} c_{j,\downarrow} c_{j,\uparrow}, \quad (1)$$

where $V_j = V_0 \cos(2\pi j/q + \phi)$ denotes a commensurate superlattice potential with the modulation period determined by q and phase ϕ , $c_{j,\sigma}^{\dagger}$ is the fermionic creation operator with spin σ , $n_{j,\sigma} = c_{j,\sigma}^{\dagger} c_{j,\sigma}$ is the

on-site particle number operator, U denotes the on-site interaction strength, and α induces nonreciprocal hopping.

In the absence of on-site interactions (see Sec. I in Ref. [94]), the single-particle energy spectrum of a 1D superlattice is split into q subbands, and the insulator with the fully filled subband exhibits a topological phase characterized by the Chern number when ϕ is taken as an additional dimension [95]. Moreover, the Hermitian superlattice system supports topological Mott phases under the strong interaction for both fermions and bosons [96–99]. In this paper, we discuss the strongly correlated topological phases in the non-Hermitian case.

We consider a spin-1/2 fermionic chain of L sites, with fractional filling factors $v_\sigma = N_\sigma/N_{\text{cell}} = 1/2$. Here N_σ is the number of fermions with spin σ , and $N_{\text{cell}} = L/q$ is the number of primitive cells. Due to half-filling at the lowest subband, the system is topologically trivial at the single-particle level. In the presence of the on-site interaction, we calculate both the charge gap Δ_c and spin gap Δ_s , which are defined as $2\Delta_c = E_0(N_\uparrow, N_\downarrow + 1) + E_0(N_\uparrow, N_\downarrow - 1) - 2E_0(N_\uparrow, N_\downarrow)$, and $2\Delta_s = E_0(N_\uparrow - 1, N_\downarrow + 1) + E_0(N_\uparrow + 1, N_\downarrow - 1) - 2E_0(N_\uparrow, N_\downarrow)$. Here E_0 is the ground-state energy, defined as the minimum real part of the many-body energy spectrum [82, 100].

Figure 1(a) plots the charge and spin gaps versus the on-site interaction strength U . In the noninteracting limit, the lowest subband is only partially filled for $v_\sigma = 1/2$; therefore, the charge gap is zero. Once the interaction is introduced, the repulsion between the two spin components forces the fermions with different spins to occupy the individual energy level of the lowest subband. Consequently, a charge gap is opened, and the non-Hermitian metallic system becomes a Mott insulator. In contrast, the spin modes are always gapless.

Moreover, the charge gap is opened even for a very small value of U , as the similar case for the Hubbard model without the superlattice potential [101]. The charge gap rises rapidly as U increases, and eventually tends to a finite value. For the Hermitian case, the charge gap tends to $\Delta_b/2$ for large U [97], where Δ_b is the single-particle gap at the 1/3 particle filling; while the saturated charge gap in the non-Hermitian case is well below this value ($\Delta_b/2 = 0.54$) due to the nonreciprocal hopping.

Many-body spectrum.—To address whether the non-Hermitian Mott insulator is topologically nontrivial, we calculate the low-energy spectra of neutral excitations in the many-excitation subspace considering both periodic and open boundaries, as summarized in Fig. 2. For the weak repulsive interaction, e.g., $U = 1$, there are no gaps for both periodic [see Fig. 2(a)] and open [see Fig. 2(b)] boundaries, and no gapless neutral excitations are thus observed. However, in the strong repulsive limit, e.g., $U = 10$ and $U = 100$, the lower-energy sector and higher-excited levels cross at $\phi = 2\pi/3$ in the

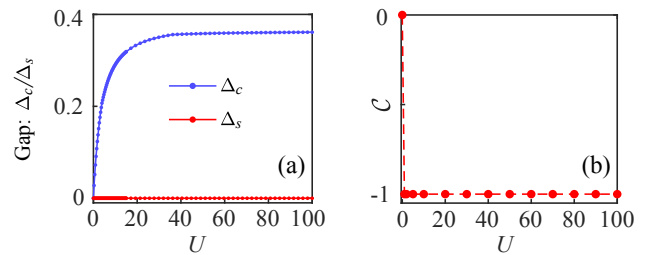


FIG. 1. (a) Charge gap Δ_c and spin gap Δ_s versus the interaction strength U for periodic boundary, with parameters $L = 12$, $N_\uparrow = 2$, $N_\downarrow = 2$, $t = 1$, $V_0 = 1.5$, $q = 3$, $\phi = 2\pi/3$, and $\alpha = 0.4$. (b) Chern number \mathcal{C} versus U , with $\alpha = 0$, and $L = 18$.

bulk gap regime, and gapless neutral excitations emerge for open boundaries [see Figs. 2(d,f)]. Note that the lower-energy sector contains six energy levels (i.e., six kinds of spin configurations) and will become degenerate in the infinite- U limit. Its degeneracy is lifted for a finite value due to spin fluctuations. For periodic-system energy spectra in Figs. 2(c,e), even in the large- U limit, no gap is opened between the lower-energy sector and higher-excited levels, due to the strong nonreciprocal hopping with $\alpha = 0.4$ (see also the eigenenergies on the complex plane in Sec. II(A) of [94]). This indicates that the energy spectrum of the non-Hermitian interacting system is sensitive to the boundary conditions, which is a manifestation of the *non-Hermitian skin effect*. Note that the periodic-system energy spectrum is gapped for the weak nonreciprocal hopping $\alpha = 0.2$ (see Sec. II(A) in [94]). In addition, the energy spectrum is always real for open boundaries. This can be seen via the similarity transformations $c_{j,\sigma} \rightarrow e^{j\alpha} c_{j,\sigma}$ and $c_{j,\sigma}^\dagger \rightarrow e^{-j\alpha} c_{j,\sigma}^\dagger$, which map the non-Hermitian Hamiltonian \mathcal{H} in Eq. (1) onto the Hermitian one.

To explore the edge localization of the gapless neutral excitation, we calculate its spatial charge and spin distributions. Note that the non-Hermitian Hamiltonian holds different left and right eigenvectors, which are defined as $\mathcal{H}^\dagger |\Phi\rangle_L = E^* |\Phi\rangle_L$, and $\mathcal{H} |\Phi\rangle_R = E |\Phi\rangle_R$. They satisfy the biorthogonal normalization condition ${}_L\langle\Phi|_R = 1$. As such, the spatial charge and spin distributions can be calculated via either biorthogonal eigenvectors or only right eigenvectors. In order to detect the non-Hermitian skin effect, as observed in the single-particle model, we adopt the right eigenvectors, where the spatial charge and spin distributions are defined as

$$\Delta n_{RR,j}^{\text{ne}} = \frac{{}_R\langle\Phi_1(N_\uparrow, N_\downarrow)|n_j|\Phi_1(N_\uparrow, N_\downarrow)\rangle_R}{{}_R\langle\Phi_1(N_\uparrow, N_\downarrow)|\Phi_1(N_\uparrow, N_\downarrow)\rangle_R} - \frac{{}_R\langle\Phi_0(N_\uparrow, N_\downarrow)|n_j|\Phi_0(N_\uparrow, N_\downarrow)\rangle_R}{{}_R\langle\Phi_0(N_\uparrow, N_\downarrow)|\Phi_0(N_\uparrow, N_\downarrow)\rangle_R}, \quad (2)$$

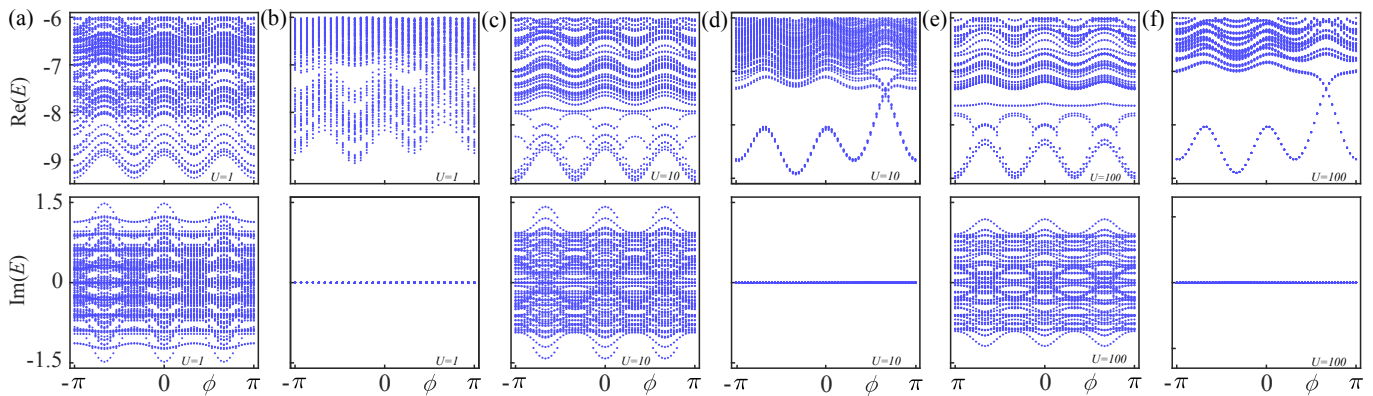


FIG. 2. Low-energy spectra versus the modulation phase ϕ for: (a,b) $U = 1$, (c,d) $U = 10$, and (e,f) $U = 100$. The spectra in (a,c,e) are for periodic boundary, and (b,d,f) for open boundaries. The parameters used here are: $L = 12$, $N_\uparrow = 2$, $N_\downarrow = 2$, $t = 1$, $V_0 = 1.5$, $q = 3$, and $\alpha = 0.4$.

$$\Delta S_{RR,j}^{\text{ne}} = \frac{{}_R \langle \Phi_1(N_\uparrow, N_\downarrow) | S_j | \Phi_1(N_\uparrow, N_\downarrow) \rangle_R - {}_R \langle \Phi_1(N_\uparrow, N_\downarrow) | \Phi_1(N_\uparrow, N_\downarrow) \rangle_R}{{}_R \langle \Phi_0(N_\uparrow, N_\downarrow) | S_j | \Phi_0(N_\uparrow, N_\downarrow) \rangle_R} - \frac{{}_R \langle \Phi_0(N_\uparrow, N_\downarrow) | \Phi_0(N_\uparrow, N_\downarrow) \rangle_R}{{}_R \langle \Phi_0(N_\uparrow, N_\downarrow) | \Phi_0(N_\uparrow, N_\downarrow) \rangle_R}, \quad (3)$$

where $n_j = n_{j,\uparrow} + n_{j,\downarrow}$, $S_j = (n_{j,\uparrow} - n_{j,\downarrow})/2$, the superscript “ne” refers to neutral, and $|\Phi_0(N_\uparrow, N_\downarrow)\rangle_R$ ($|\Phi_1(N_\uparrow, N_\downarrow)\rangle_R$) is the right lowest (higher) energy state. The above two equations provide the differences of density and magnetization distributions of two in-gap modes in the upper and lower branches. According to Figs. 3(a,b), the gapless neutral excitation only carries a charge degree of freedom at the edges. Moreover, only the in-gap states with $\phi < 2\pi/3$ exhibit edge excitations for $\alpha = 0.4$ and $V_0 = 1.5$ [see Fig. 3(a)]. In contrast, for $\alpha = -0.4$, edge excitations emerge only if $\phi > 2\pi/3$, as shown in Fig. 3(c) (see also the results for $U = 10$ in Sec. II(B) of [94]). Therefore, the charge distributions calculated by only the right eigenvectors indicate that the non-Hermitian interacting system shows the anomalous boundary effect, where some in-gap states exhibit no edge excitations in the open chain. However, this phenomenon is absent for the non-Hermitian single-particle case (see Sec. I in [94]). Moreover, such an anomalous boundary effect disappears for weak nonreciprocal hopping, i.e., $\alpha = 0.2$, as shown in Fig. 3(d), or large modulation amplitude, i.e., $V_0 = 4$ in Fig. 3(e). These indicate that *the anomalous boundary effect results from the combined effects of the nonreciprocal hopping, superlattice potential, and interactions*. The interactions drive the metallic phase into a topological insulator, the superlattice potential forces particles to occupy the site with lower potential in the ground state, and the nonreciprocal hopping pushes particles accumulated towards one of two ends in the higher-excited state. These lead to the absence of neutral excitations at the edges for certain values of ϕ (for detailed explanations, see Sec. II(C) of [94]).

Furthermore, unlike the single-particle model (see Sec. I in [94]), the nonreciprocal hopping here does not cause bulk charges to accumulate near the boundaries due to the Pauli exclusion principle and interactions [see Fig. 3(f)].

The charge distributions computed by only the right eigenvectors lead to the absence of edge excitations for some in-gap states due to the intrinsic non-Hermitian skin effect. The edge excitations can be restored by considering the biorthogonal eigenvectors, where the charge distribution is calculated as

$$\Delta n_{LR,j}^{\text{ne}} = {}_L \langle \Phi_1(N_\uparrow, N_\downarrow) | n_j | \Phi_1(N_\uparrow, N_\downarrow) \rangle_R - {}_L \langle \Phi_0(N_\uparrow, N_\downarrow) | n_j | \Phi_0(N_\uparrow, N_\downarrow) \rangle_R. \quad (4)$$

As shown in Fig. 4, all the in-gap states of the neutral excitations are localized at the edges. In addition, the charge distributions with $\alpha = 0.4$ [see Fig. 4(a)] are the same as the ones with $\alpha = -0.4$ [see Fig. 4(b)], indicating that they are insensitive to the nonreciprocal hopping based on the biorthogonal formula.

Quasiparticle spectrum.—To further explore the topological properties of the Mott insulator, we proceed to calculate the quasiparticle energy spectrum, or charge excitation spectrum, defined as $\Delta E_c(N_\uparrow, N_\downarrow) = E_0(N_\uparrow, N_\downarrow + 1) - E_0(N_\uparrow, N_\downarrow)$. The corresponding spatial charge distribution, calculated by both only the right eigenvectors and biorthogonal eigenvectors, are:

$$\Delta n_{RR,j}^c = \frac{{}_R \langle \Phi_0(N_\uparrow, N_\downarrow + 1) | n_j | \Phi_0(N_\uparrow, N_\downarrow + 1) \rangle_R - {}_R \langle \Phi_0(N_\uparrow, N_\downarrow + 1) | \Phi_0(N_\uparrow, N_\downarrow + 1) \rangle_R}{{}_R \langle \Phi_0(N_\uparrow, N_\downarrow) | n_j | \Phi_0(N_\uparrow, N_\downarrow) \rangle_R} - \frac{{}_R \langle \Phi_0(N_\uparrow, N_\downarrow) | \Phi_0(N_\uparrow, N_\downarrow) \rangle_R}{{}_R \langle \Phi_0(N_\uparrow, N_\downarrow) | \Phi_0(N_\uparrow, N_\downarrow) \rangle_R}, \quad (5)$$

$$\Delta n_{LR,j}^c = {}_L \langle \Phi_0(N_\uparrow, N_\downarrow + 1) | n_j | \Phi_0(N_\uparrow, N_\downarrow + 1) \rangle_R - {}_L \langle \Phi_0(N_\uparrow, N_\downarrow) | n_j | \Phi_0(N_\uparrow, N_\downarrow) \rangle_R, \quad (6)$$

Figures 5(a,b) plot the charge excitation spectra versus the modulation phase ϕ under both periodic and open

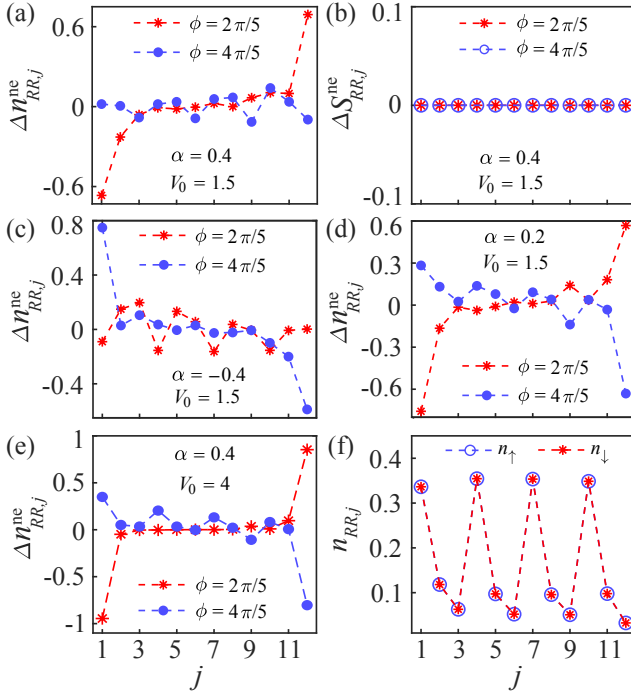


FIG. 3. Spatial distributions of the (a,c,d,e) charge and (b) spin for the neutral excitation modes, calculated via only the right eigenvectors, for different modulation phases ϕ . The spatial distributions are calculated for: (a,b) $\alpha = 0.4$, $V_0 = 1.5$; (c) $\alpha = -0.4$, $V_0 = 1.5$; (d) $\alpha = 0.2$, $V_0 = 1.5$; and (e) $\alpha = 0.4$, $V_0 = 4$. (f) Spin-resolved charge densities of the ground state for $\phi = 2\pi/5$, $\alpha = 0.4$ and $V_0 = 1.5$. Same parameters as in Fig. 2.

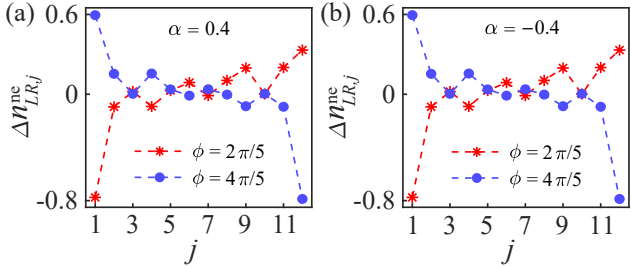


FIG. 4. Spatial charge distributions, calculated via biorthogonal eigenvectors, of the neutral excitations for (a) $\alpha = 0.4$ and (b) $\alpha = -0.4$. Same parameters as in Fig. 2.

boundaries for $\Delta E_c(N_\uparrow = 2, N_\downarrow = 2)$ and $\Delta E_c(N_\uparrow = 2, N_\downarrow = 1)$. For periodic boundary, the charge excitation spectrum is gapped. Once the boundary is opened, the in-gap modes appear.

To explore the non-Hermitian skin effect on edge charge excitations, Figure 5(c,d,e) shows the spatial charge distributions calculated using only the right eigenvector. As the same case of neutral excitations, only the in-gap modes of the charge excitations with $\phi < 2\pi/3$ are localized at the edges for strong nonreciprocal hopping, i.e., $\alpha = 0.4$ in Fig. 5(c). This

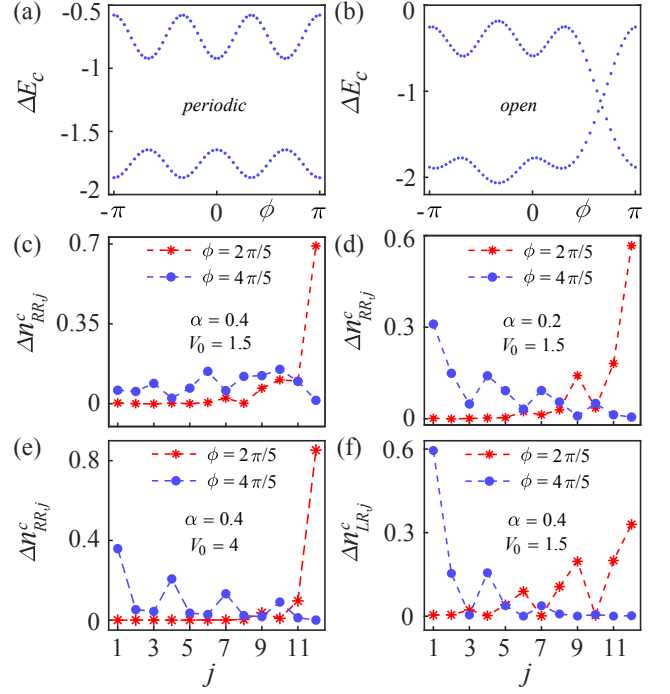


FIG. 5. Charge excitation spectra $\Delta E_c(2,2)$ and $\Delta E_c(2,1)$ versus the modulation phase ϕ for (a) periodic and (b) open boundaries. Spatial charge distributions, calculated using only the right eigenvectors, of the charge excitations for: (c) $\alpha = 0.4$, $V_0 = 1.5$; (d) $\alpha = 0.2$, $V_0 = 1.5$; and (e) $\alpha = 0.4$, $V_0 = 4$. (f) Spatial charge distributions calculated using biorthogonal eigenvectors. Same parameters as in Fig. 2.

anomalous boundary effect is due to the combined results of nonreciprocal hopping, superlattice potential, and interactions (for detailed explanations, see Sec. II(C) of [94]). Note that such an anomalous boundary effect disappears for small α [see Fig. 5(d)] or large V_0 [see Fig. 5(e)]. To fully characterize boundary charge excitations, we can implement biorthogonal eigenvectors, where all the in-gap modes show edge excitations [see Fig. 5(f)].

In addition to the case for the filling factors $v_\uparrow = v_\downarrow = 1/2$ discussed here, as long as the lowest subband of the non-Hermitian superlattice system is half-filled with $v_\uparrow + v_\downarrow = 1$, the interaction can drive it into the topological Mott insulator, which shows anomalous boundary effects (see the results for $v_\uparrow = 1/5$ and $v_\downarrow = 4/5$ in Sec. II(D) of [94]). Note that the superlattice model with purely imaginary-valued interactions can also drive the metallic system into a topological Mott insulator, where the effective repulsion is created by the continuous quantum Zeno effect, but this model shows no anomalous boundary effects due to the absence of the non-Hermitian skin effect (see Sec. III in [94]).

Topological invariant.—To characterize the topological feature of the system considered, we compute the many-

body Chern number, which is defined as:

$$C = \frac{1}{2\pi} \int_{-\pi}^{\pi} d\theta \int_{-\pi}^{\pi} d\phi (\partial_{\theta} A_{\phi} - \partial_{\phi} A_{\theta}), \quad (7)$$

where the Berry connection $A_{\mu} = i_L \langle \Psi_g | \partial_{\mu} | \Psi_g \rangle_R$ ($\mu = \theta, \phi$). $|\Psi_g\rangle_R$ ($|\Psi_g\rangle_L$) is the many-body right (left) ground state under the twist boundary conditions $c_{j+L,\sigma} = e^{i\theta} c_{j,\sigma}$, with twist angle θ . Due to the nonreciprocal hopping, the Chern number based on the Hamiltonian \mathcal{H} in Eq. (1) fails to characterize the bulk-boundary correspondence. The non-Hermitian Hamiltonian \mathcal{H} can be mapped onto a Hermitian one via a similarity transformation, and they share the same quasiparticle bands for open boundaries. Thus, we can restore the bulk-boundary correspondence by computing the Chern number of the corresponding Hermitian Hamiltonian under its twisted boundary condition. Figure 1(b) plots the topological phase diagram with $\alpha = 0$, where $C = -1$ even for very small U , because an arbitrary small repulsive interaction [see also Fig. 1(a)] can drive the Hubbard system into topological Mott phases [97, 101].

Summary and discussion.—We have discussed topological properties of an interaction-induced topological Mott insulator in a 1D non-Hermitian spinful fermionic superlattice system. We analyzed its low-energy neutral and charge excitations spectra in the presence of nonreciprocal hopping, where in-gap modes appear. We found that the nonreciprocal hopping makes the neutral excitation spectrum sensitive to the boundary conditions, which is a manifestation of the non-Hermitian skin effect. The interplay of nonreciprocal hopping, superlattice potential, and interactions leads to the absence of edge excitations, defined by only the right eigenvectors, of some in-gap modes appearing in both the neutral and charge excitation spectra. Moreover, these edge excitations can be characterized by using biorthogonal eigenvectors.

The non-Hermitian skin effect has been shown to cause unusual properties in fermionic many-body systems, i.e., a Fermi surface in real space [102]. Our findings indicate that the non-Hermitian skin effect, in combination with a periodic modulation and interactions, can lead to unconventional topological features without Hermitian counterparts, which is worth further exploration. Possible future research directions include non-Hermitian fractional quantum Hall effect [103], fractional charge pumping [104], and an extension to higher-dimensional systems [105]. Meanwhile, we hope that our studies inspire further future explorations of the role of the non-Hermitian skin effect and searching for novel topological features in non-Hermitian interacting fermionic systems.

Noted added: After this work was completed, we became aware of two related works [106, 107], which discuss non-Hermitian topological Mott insulators of interacting bosons. Unlike the fermionic model considered here, the

nonreciprocal bosonic model exhibits the accumulation of particle density at the edges, and no anomalous boundary effect is reported [106].

T.L. is grateful to Zhong Wang, Haiping Hu, Clemens Gneiting and Zhihao Xu for valuable discussions. T.L. acknowledges support from the Grant-in-Aid for a JSPS Foreign Postdoctoral Fellowship (P18023). T.Y. is supported by JSPS KAKENHI (Grants No. JP19K21032). Z.L.X thanks the support from the NSFC (Grant No. 11874432). F.N. is supported in part by: NTT Research, Army Research Office (ARO) (Grant No. W911NF-18-1-0358), Japan Science and Technology Agency (JST) (via the CREST Grant No. JPMJCR1676), Japan Society for the Promotion of Science (JSPS) (via the KAKENHI Grant No. JP20H00134, and the grant JSPS-RFBR Grant No. JPJSBP120194828), and the Grant No. FQXi-IAF19-06 from the Foundational Questions Institute Fund (FQXi), a donor advised fund of the Silicon Valley Community Foundation.

* E-mail: tao.liu@riken.jp

† E-mail: fnori@riken.jp

- [1] M. S. Rudner and L. S. Levitov, “Topological transition in a non-Hermitian quantum walk,” *Phys. Rev. Lett.* **102**, 065703 (2009).
- [2] K. Esaki, M. Sato, K. Hasebe, and M. Kohmoto, “Edge states and topological phases in non-Hermitian systems,” *Phys. Rev. B* **84**, 205128 (2011).
- [3] S. Malzard, C. Poli, and H. Schomerus, “Topologically protected defect states in open photonic systems with non-Hermitian charge-conjugation and parity-time symmetry,” *Phys. Rev. Lett.* **115**, 200402 (2015).
- [4] S. Weimann, M. Kremer, Y. Plotnik, Y. Lumer, S. Nolte, K. G. Makris, M. Segev, M. C. Rechtsman, and A. Szameit, “Topologically protected bound states in photonic paritytime-symmetric crystals,” *Nat. Mater.* **16**, 433 (2016).
- [5] T. E. Lee, “Anomalous edge state in a non-Hermitian lattice,” *Phys. Rev. Lett.* **116**, 133903 (2016).
- [6] Y. Xu, S. T. Wang, and L. M. Duan, “Weyl exceptional rings in a three-dimensional dissipative cold atomic gas,” *Phys. Rev. Lett.* **118**, 045701 (2017).
- [7] D. Leykam, K. Y. Bliokh, C. Huang, Y. D. Chong, and F. Nori, “Edge modes, degeneracies, and topological numbers in non-Hermitian systems,” *Phys. Rev. Lett.* **118**, 040401 (2017).
- [8] H. Shen, B. Zhen, and L. Fu, “Topological band theory for non-Hermitian Hamiltonians,” *Phys. Rev. Lett.* **120**, 146402 (2018).
- [9] V. M. Martinez Alvarez, J. E. Barrios Vargas, and L. E. F. Foa Torres, “Non-Hermitian robust edge states in one dimension: Anomalous localization and eigenspace condensation at exceptional points,” *Phys. Rev. B* **97**, 121401 (2018).
- [10] G. Harari, M. A. Bandres, Y. Lumer, M. C. Rechtsman, Y. D. Chong, M. Khajavikhan, D. N. Christodoulides, and M. Segev, “Topological insulator laser: Theory,”

- Science* **359**, 6381 (2018).
- [11] M. A. Bandres, S. Wittek, G. Harari, M. Parto, J. Ren, M. Segev, D. N. Christodoulides, and M. Khajavikhan, “Topological insulator laser: Experiments,” *Science* **359**, 6381 (2018).
- [12] H. Zhou, C. Peng, Y. Yoon, C. W. Hsu, K. A. Nelson, L. Fu, J. D. Joannopoulos, M. Soljačić, and B. Zhen, “Observation of bulk Fermi arc and polarization half charge from paired exceptional points,” *Science* **359**, 1009 (2018).
- [13] X. Ye, “Why does bulk boundary correspondence fail in some non-Hermitian topological models,” *J. Phys. Commun.* **2**, 035043 (2018).
- [14] M. Pan, H. Zhao, P. Miao, S. Longhi, and L. Feng, “Photonic zero mode in a non-Hermitian photonic lattice,” *Nat. Commun.* **9**, 1308 (2018).
- [15] Z. Gong, Y. Ashida, K. Kawabata, K. Takasan, S. Higashikawa, and M. Ueda, “Topological phases of non-Hermitian systems,” *Phys. Rev. X* **8**, 031079 (2018).
- [16] Y. Chen and H. Zhai, “Hall conductance of a non-Hermitian Chern insulator,” *Phys. Rev. B* **98**, 245130 (2018).
- [17] F. K. Kunst, E. Edvardsson, J. C. Budich, and E. J. Bergholtz, “Biorthogonal bulk-boundary correspondence in non-Hermitian systems,” *Phys. Rev. Lett.* **121**, 026808 (2018).
- [18] S. Yao and Z. Wang, “Edge states and topological invariants of non-Hermitian systems,” *Phys. Rev. Lett.* **121**, 086803 (2018).
- [19] S. Yao, F. Song, and Z. Wang, “Non-Hermitian Chern bands,” *Phys. Rev. Lett.* **121**, 136802 (2018).
- [20] K. Kawabata, K. Shiozaki, and M. Ueda, “Anomalous helical edge states in a non-Hermitian Chern insulator,” *Phys. Rev. B* **98**, 165148 (2018).
- [21] Z. Y. Ge, Y. R. Zhang, T. Liu, S. W. Li, H. Fan, and F. Nori, “Topological band theory for non-Hermitian systems from the Dirac equation,” *Phys. Rev. B* **100**, 054105 (2019).
- [22] K. Kawabata, S. Higashikawa, Z. Gong, Y. Ashida, and M. Ueda, “Topological unification of time-reversal and particle-hole symmetries in non-Hermitian physics,” *Nat. Commun.* **10**, 297 (2019).
- [23] C. H. Lee and R. Thomale, “Anatomy of skin modes and topology in non-Hermitian systems,” *Phys. Rev. B* **99**, 201103 (2019).
- [24] H. Zhou and J. Y. Lee, “Periodic table for topological bands with non-Hermitian symmetries,” *Phys. Rev. B* **99**, 235112 (2019).
- [25] K. Kawabata, K. Shiozaki, M. Ueda, and M. Sato, “Symmetry and topology in non-Hermitian physics,” *Phys. Rev. X* **9**, 041015 (2019).
- [26] C. H. Liu and S. Chen, “Topological classification of defects in non-Hermitian systems,” *Phys. Rev. B* **100**, 144106 (2019).
- [27] T. S. Deng and W. Yi, “Non-Bloch topological invariants in a non-Hermitian domain wall system,” *Phys. Rev. B* **100**, 035102 (2019).
- [28] T. Liu, Y. R. Zhang, Q. Ai, Z. Gong, K. Kawabata, M. Ueda, and F. Nori, “Second-order topological phases in non-Hermitian systems,” *Phys. Rev. Lett.* **122**, 076801 (2019).
- [29] F. Song, S. Yao, and Z. Wang, “Non-Hermitian topological invariants in real space,” *Phys. Rev. Lett.* **123**, 246801 (2019).
- [30] F. Song, S. Yao, and Z. Wang, “Non-Hermitian skin effect and chiral damping in open quantum systems,” *Phys. Rev. Lett.* **123**, 170401 (2019).
- [31] A. Ghatak and T. Das, “New topological invariants in non-Hermitian systems,” *J. Phys. Condens. Matter* **31**, 263001 (2019).
- [32] T. Yoshida, R. Peters, N. Kawakami, and Y. Hatsugai, “Symmetry-protected exceptional rings in two-dimensional correlated systems with chiral symmetry,” *Phys. Rev. B* **99**, 121101 (2019).
- [33] K. Kawabata, T. Bessho, and M. Sato, “Classification of exceptional points and non-Hermitian topological semimetals,” *Phys. Rev. Lett.* **123**, 066405 (2019).
- [34] N. Okuma and M. Sato, “Topological phase transition driven by infinitesimal instability: Majorana fermions in non-Hermitian spintronics,” *Phys. Rev. Lett.* **123**, 097701 (2019).
- [35] N. Okuma, K. Kawabata, K. Shiozaki, and M. Sato, “Topological origin of non-Hermitian skin effects,” arXiv:1910.02878 (2019).
- [36] Q. B. Zeng, Y. B. Yang, and Y. Xu, “Topological phases in non-Hermitian Aubry-Andr-Harper models,” arXiv:1901.08060 (2019).
- [37] C. H. Lee, L. Li, and J. Gong, “Hybrid higher-order skin-topological modes in nonreciprocal systems,” *Phys. Rev. Lett.* **123**, 016805 (2019).
- [38] E. Edvardsson, F. K. Kunst, and E. J. Bergholtz, “Non-Hermitian extensions of higher-order topological phases and their biorthogonal bulk-boundary correspondence,” *Phys. Rev. B* **99**, 081302 (2019).
- [39] K. Yokomizo and S. Murakami, “Non-Bloch band theory of non-Hermitian systems,” *Phys. Rev. Lett.* **123**, 066404 (2019).
- [40] X. W. Luo and C. Zhang, “Higher-order topological corner states induced by gain and loss,” *Phys. Rev. Lett.* **123**, 073601 (2019).
- [41] S. Longhi, “Probing non-Hermitian skin effect and non-Bloch phase transitions,” *Phys. Rev. Research* **1**, 023013 (2019).
- [42] M. Ezawa, “Non-Hermitian higher-order topological states in nonreciprocal and reciprocal systems with their electric-circuit realization,” *Phys. Rev. B* **99**, 201411 (2019).
- [43] L. Zhou, “Dynamical characterization of non-Hermitian Floquet topological phases in one dimension,” *Phys. Rev. B* **100**, 184314 (2019).
- [44] X. M. Yang, P. Wang, L. Jin, and Z. Song, “Visualizing topology of real-energy gapless phase arising from exceptional point,” arXiv:1905.07109 (2019).
- [45] T. Ohashi, S. Kobayashi, and Y. Kawaguchi, “Generalized Berry phase for a bosonic Bogoliubov system with exceptional points,” arXiv:1904.08724 (2019).
- [46] X. Yang, Y. Cao, and Y. Zhai, “Non-Hermitian Weyl semimetals: Non-Hermitian skin effect and non-Bloch bulk-boundary correspondence,” arXiv:1904.02492 (2019).
- [47] K. L. Zhang, H. C. Wu, L. Jin, and Z. Song, “Topological phase transition independent of system non-Hermiticity,” *Phys. Rev. B* **100**, 045141 (2019).
- [48] J. Hou, Y. J. Wu, and C. Zhang, “Two-dimensional non-Hermitian topological phases induced by asymmetric hopping in a one-dimensional superlattice,” arXiv:1906.03988 (2019).
- [49] J. Y. Lee, J. Ahn, H. Zhou, and A. Vishwanath,

- “Topological correspondence between Hermitian and non-Hermitian systems: Anomalous dynamics,” *Phys. Rev. Lett.* **123**, 206404 (2019).
- [50] H. C. Wu, L. Jin, and Z. Song, “Inversion symmetric non-Hermitian Chern insulator,” *Phys. Rev. B* **100**, 155117 (2019).
- [51] A. Y. Song, X. Q. Sun, A. Dutt, M. Minkov, C. Wojcik, H. Wang, I. Williamson, M. Orenstein, and S. Fan, “ \mathcal{PT} -symmetric topological edge-gain effect,” arXiv:1910.10946 (2019).
- [52] H. Zhao, X. Qiao, T. Wu, B. Midya, S. Longhi, and L. Feng, “Non-Hermitian topological light steering,” *Science* **365**, 1163 (2019).
- [53] T. Yoshida, T. Mizoguchi, and Y. Hatsugai, “Mirror skin effect and its electric circuit simulation,” arXiv:1912.12022 (2019).
- [54] X. R. Wang, C. X. Guo, and S. P. Kou, “Defective edge states and anomalous bulk-boundary correspondence in non-Hermitian topological systems,” arXiv:1912.04024 (2019).
- [55] H. G. Zirnstein, G. Refael, and B. Rosenow, “Bulk-boundary correspondence for non-Hermitian Hamiltonians via Green functions,” arXiv:1901.11241 (2019).
- [56] E. S. Borgnia, A. J. Kruchkov, and R. J. Slager, “Non-Hermitian boundary modes,” arXiv:1902.07217 (2019).
- [57] E. Lee, H. Lee, and B. J. Yang, “Many-body approach to non-Hermitian physics in fermionic systems,” arXiv:1912.05825 (2019).
- [58] E. J. Bergholtz, J. C. Budich, and F. K. Kunst, “Exceptional topology of non-Hermitian systems,” arXiv:1912.10048 (2019).
- [59] W. Xi, Z. H. Zhang, Z. C. Gu, and W. Q. Chen, “Classification of topological phases in one dimensional interacting non-Hermitian systems and emergent unitarity,” arXiv:1911.01590 (2019).
- [60] K. G. Makris, R. El-Ganainy, D. N. Christodoulides, and Z. H. Musslimani, “Beam dynamics in \mathcal{PT} symmetric optical lattices,” *Phys. Rev. Lett.* **100**, 103904 (2008).
- [61] Y. D. Chong, L. Ge, and A. D. Stone, “ \mathcal{PT} -symmetry breaking and laser-absorber modes in optical scattering systems,” *Phys. Rev. Lett.* **106**, 093902 (2011).
- [62] A. Regensburger, C. Bersch, M. A. Miri, G. Onishchukov, D. N. Christodoulides, and U. Peschel, “Paritytime synthetic photonic lattices,” *Nature* **488**, 167 (2012).
- [63] H. Jing, S. K. Özdemir, X. Y. Lü, J. Zhang, L. Yang, and F. Nori, “ \mathcal{PT} -symmetric phonon laser,” *Phys. Rev. Lett.* **113**, 053604 (2014).
- [64] H. Hodaei, M. A. Miri, M. Heinrich, D. N. Christodoulides, and M. Khajavikhan, “Parity-time-symmetric microring lasers,” *Science* **346**, 975 (2014).
- [65] B. Peng, S. K. Özdemir, F. Lei, F. Monifi, M. Gianfreda, G. L. Long, S. Fan, F. Nori, C. M. Bender, and L. Yang, “Paritytime-symmetric whispering-gallery microcavities,” *Nat. Phys.* **10**, 394 (2014).
- [66] L. Feng, Z. J. Wong, R. M. Ma, Y. Wang, and X. Zhang, “Single-mode laser by parity-time symmetry breaking,” *Science* **346**, 972 (2014).
- [67] B. Peng, S. K. Özdemir, S. Rotter, H. Yilmaz, M. Liertzer, F. Monifi, C. M. Bender, F. Nori, and L. Yang, “Loss-induced suppression and revival of lasing,” *Science* **346**, 328 (2014).
- [68] H. Jing, S. K. Özdemir, Z. Geng, J. Zhang, X. Y. Lü, B. Peng, L. Yang, and F. Nori, “Optomechanically-induced transparency in parity-time-symmetric microresonators,” *Sci. Rep.* **5**, 9663 (2015).
- [69] Z. P. Liu, J. Zhang, S. K. Özdemir, B. Peng, H. Jing, X. Y. Lü, C. W. Li, L. Yang, F. Nori, and Y. X. Liu, “Metrology with \mathcal{PT} -symmetric cavities: Enhanced sensitivity near the \mathcal{PT} -phase transition,” *Phys. Rev. Lett.* **117**, 110802 (2016).
- [70] K. Kawabata, Y. Ashida, and M. Ueda, “Information retrieval and criticality in parity-time-symmetric systems,” *Phys. Rev. Lett.* **119**, 190401 (2017).
- [71] H. Jing, S. K. Özdemir, H. Lü, and F. Nori, “High-order exceptional points in optomechanics,” *Sci. Rep.* **7**, 3386 (2017).
- [72] H. Lü, S. K. Özdemir, L. M. Kuang, F. Nori, and H. Jing, “Exceptional points in random-defect phonon lasers,” *Phys. Rev. Applied* **8**, 044020 (2017).
- [73] R. El-Ganainy, K. G. Makris, M. Khajavikhan, Z. H. Musslimani, S. Rotter, and D. N. Christodoulides, “Non-Hermitian physics and PT symmetry,” *Nat. Phys.* **14**, 11 (2018).
- [74] J. Zhang, B. Peng, S. K. Özdemir, K. Pichler, D. O. Krimer, G. Zhao, F. Nori, Y. X. Liu, S. Rotter, and L. Yang, “A phonon laser operating at an exceptional point,” *Nat. Photon.* **12**, 479 (2018).
- [75] W. T. Xue, M. R. Li, Y. M. Hu, F. Song, and Z. Wang, “Non-Hermitian band theory of directional amplification,” arXiv:2004.09529 (2020).
- [76] V. Kozii and L. Fu, “Non-Hermitian topological theory of finite-lifetime quasiparticles: Prediction of bulk Fermi arc due to exceptional point,” arXiv:1708.05841 (2017).
- [77] H. Shen and L. Fu, “Quantum oscillation from in-gap states and non-Hermitian Landau level problem,” *Phys. Rev. Lett.* **121**, 026403 (2018).
- [78] A. A. Zyuzin and A. Yu. Zyuzin, “Flat band in disorder-driven non-Hermitian Weyl semimetals,” *Phys. Rev. B* **97**, 041203 (2018).
- [79] M. Papaj, H. Isobe, and L. Fu, “Nodal arc of disordered Dirac fermions and non-Hermitian band theory,” *Phys. Rev. B* **99**, 201107 (2019).
- [80] T. Yoshida, R. Peters, and N. Kawakami, “Non-Hermitian perspective of the band structure in heavy-fermion systems,” *Phys. Rev. B* **98**, 035141 (2018).
- [81] M. Naghiloo, M. Abbasi, Yogesh N. Joglekar, and K. W. Murch, “Quantum state tomography across the exceptional point in a single dissipative qubit,” *Nat. Phys.* **15**, 1232 (2019).
- [82] T. Yoshida, K. Kudo, and Y. Hatsugai, “Non-Hermitian fractional quantum Hall states,” *Sci. Rep.* **9**, 16895 (2019).
- [83] D. N. Sheng, Z. C. Gu, K. Sun, and L. Sheng, “Fractional quantum Hall effect in the absence of Landau levels,” *Nat. Commun.* **2**, 389 (2011).
- [84] N. Regnault and B. A. Bernevig, “Fractional Chern insulator,” *Phys. Rev. X* **1**, 021014 (2011).
- [85] E. J. Bergholtz and Z. Liu, “Topological flat band models and fractional Chern insulators,” *Int. J. Mod. Phys. B* **27**, 1330017 (2013).
- [86] J. Maciejko and G. A. Fiete, “Fractionalized topological insulators,” *Nat. Phys.* **11**, 385 (2015).
- [87] T. Yoshida, I. Danshita, R. Peters, and N. Kawakami, “Reduction of topological \mathbb{Z} classification in cold-atom systems,” *Phys. Rev. Lett.* **121**, 025301 (2018).

- [88] S. Raghu, X. L. Qi, C. Honerkamp, and S. C. Zhang, “Topological Mott insulators,” *Phys. Rev. Lett.* **100**, 156401 (2008).
- [89] S. Rachel, “Interacting topological insulators: a review,” *Rep. Prog. Phys.* **81**, 116501 (2018).
- [90] D. Pesin and L. Balents, “Mott physics and band topology in materials with strong spin–orbit interaction,” *Nat. Phys.* **6**, 376 (2010).
- [91] T. Yoshida, R. Peters, S. Fujimoto, and N. Kawakami, “Characterization of a topological Mott insulator in one dimension,” *Phys. Rev. Lett.* **112**, 196404 (2014).
- [92] K. Kudo, T. Yoshida, and Y. Hatsugai, “Higher-order topological Mott insulators,” *Phys. Rev. Lett.* **123**, 196402 (2019).
- [93] There is another phase called topological Mott insulator, where correlated fermions mimic gapless edge modes of bosonic symmetry-protected topological phases. Note that this type of phases differs from the non-Hermitian topological Mott insulator discussed in this work.
- [94] See Supplemental Material for more details.
- [95] L. J. Lang, X. Cai, and S. Chen, “Edge states and topological phases in one-dimensional optical superlattices,” *Phys. Rev. Lett.* **108**, 220401 (2012).
- [96] S. L. Zhu, Z. D. Wang, Y. H. Chan, and L. M. Duan, “Topological Bose-Mott insulators in a one-dimensional optical superlattice,” *Phys. Rev. Lett.* **110**, 075303 (2013).
- [97] Z. Xu and S. Chen, “Topological Mott insulators of ultracold atomic mixtures induced by interactions in one-dimensional optical superlattices,” *Phys. Rev. B* **88**, 045110 (2013).
- [98] F. Grusdt, M. Hönig, and M. Fleischhauer, “Topological edge states in the one-dimensional superlattice Bose-Hubbard model,” *Phys. Rev. Lett.* **110**, 260405 (2013).
- [99] H. Hu, S. Chen, T. S. Zeng, and C. Zhang, “Topological Mott insulator with bosonic edge modes in one-dimensional fermionic superlattices,” *Phys. Rev. A* **100**, 023616 (2019).
- [100] Y. Ashida, S. Furukawa, and M. Ueda, “Quantum critical behavior influenced by measurement backaction in ultracold gases,” *Phys. Rev. A* **94**, 053615 (2016).
- [101] E. H. Lieb and F. Y. Wu, “Absence of Mott transition in an exact solution of the short-range, one-band model in one dimension,” *Phys. Rev. Lett.* **20**, 1445 (1968).
- [102] S. Mu, C. H. Lee, L. Li, and J. Gong, “Emergent Fermi surface in a many-body non-Hermitian fermionic chain,” arXiv:1911.00023 (2019).
- [103] Z. Xu, L. Li, and S. Chen, “Fractional topological states of dipolar fermions in one-dimensional optical superlattices,” *Phys. Rev. Lett.* **110**, 215301 (2013).
- [104] T. S. Zeng, W. Zhu, and D. N. Sheng, “Fractional charge pumping of interacting bosons in one-dimensional superlattice,” *Phys. Rev. B* **94**, 235139 (2016).
- [105] M. Lohse, C. Schweizer, H. M. Price, O. Zilberberg, and I. Bloch, “Exploring 4D quantum Hall physics with a 2D topological charge pump,” *Nature* **553**, 55 (2018).
- [106] D. W. Zhang, Y. L. Chen, G. Q. Zhang, L. J. Lang, Z. Li, and S. L. Zhu, “Skin superfluid, topological Mott insulators, and asymmetric dynamics in interacting non-Hermitian Aubry-Andre-Harper models,” arXiv:2001.07088 (2020).
- [107] Z. Xu and S. Chen, “Topological Bose-Mott insulators in one-dimensional non-Hermitian superlattices,” arXiv:2002.00554 (2020).

SUPPLEMENTAL MATERIAL FOR “NON-HERMITIAN TOPOLOGICAL MOTT INSULATORS IN 1D FERMIONIC SUPERLATTICES”

I. Single-particle spectrum

In the absence of interactions, we consider the following single-particle non-Hermitian Hamiltonian with a superlattice potential

$$\mathcal{H}_s = -t \sum_j \left(e^\alpha c_{j+1}^\dagger c_j + e^{-\alpha} c_j^\dagger c_{j+1} \right) + V_0 \sum_j \cos(2\pi j/q + \phi) n_j, \quad (\text{S1})$$

The periodic modulation [i.e., the last term in Eq. (S1)] introduces a superlattice structure, where each lattice site of the 1D chain can be now represented by two quantities: x_m denoting the position of the supercell, and β indexing the lattices inside the supercell. For a periodic system, we can transform the real-space Hamiltonian \mathcal{H}_s to the momentum-space one $\mathcal{H}_s(k)$ by the following Fourier transformation

$$c_{\beta,m} = \frac{1}{\sqrt{N_{\text{cell}}}} \sum_k c_{\beta,k} e^{-ikx_m}, \quad (\text{S2})$$

where $\beta = 1, 2, \dots, q$, $N_{\text{cell}} = L/q$, $m = 1, 2, \dots, N_{\text{cell}}$, and $-\pi/q < k < \pi/q$. Thus, the momentum-space Hamiltonian is given by

$$\begin{aligned} \mathcal{H}_s(k) = & -t \sum_k \left[e^\alpha \left(c_{2,k}^\dagger c_{1,k} + \dots + c_{q,k}^\dagger c_{q-1,k} + c_{1,k}^\dagger c_{q,k} e^{ikq} \right) + e^{-\alpha} \left(c_{1,k}^\dagger c_{2,k} + \dots + c_{q-1,k}^\dagger c_{q,k} + c_{q,k}^\dagger c_{1,k} e^{-ikq} \right) \right] \\ & + V_0 \sum_{\beta,k} \cos(2\pi j/q + \phi) n_{\beta,k}, \end{aligned} \quad (\text{S3})$$

According to Eq. (S3), the single-particle spectrum is split into q bands due to the superlattice potential, as shown by the gapped complex energy spectra for $q = 3$ using the periodic boundary condition in Figs. S1(a,b). The energy spectrum is gapped for $\alpha = 0.2$ at both the 1/3 and 2/3 particle fillings [see Fig. S1(c)]; while it is gapless for $\alpha = 0.4$ at the 1/3 particle filling [see Fig. S1(d)] due to the nonreciprocal hopping, which is different from the Hermitian case [S1].

When the single-particle chain is changed from periodic boundary to the open one, in-gap modes appear for $\alpha = 0.2$ at both the 1/3 and 2/3 particle fillings (see Figs. S1(e,f)). These in-gap modes (there exist two edge modes at a specific α) can be localized at both the left and right ends of the chain for the small nonreciprocal hopping factor $\alpha = 0.2$, as shown in Figs. S1(g,h). While, for the strong nonreciprocal hopping, i.e., $\alpha = 0.4$, the in-gap modes are localized only at the right end due to the much larger forward hopping amplitude than the backward one [see Figs. S1(i,j)], which is dubbed the *non-Hermitian skin effect*.

II. Non-Hermitian model with nonreciprocal hopping

A. Many-body spectrum for $\alpha = 0.2$

In the main text, we discuss many-body spectra for the strong nonreciprocal hopping, i.e., $\alpha = 0.4$, where the spectra of the periodic chain are gapless, and these of the open chain are gapped for the strong repulsive interactions. Here we plot the energy spectra for the weak nonreciprocal hopping $\alpha = 0.2$, as shown in Fig. S2. Similarly to the case of strong nonreciprocal hopping, the eigenenergy spectra using both the periodic and open boundary conditions are gapless for small repulsive interaction, e.g., $U = 1$ as shown in Figs. S2(a,b), and no edge excitations are thus observed. While, in contrast to the case of the strong nonreciprocal hopping [see also eigenenergies on the complex plane in Fig. S3(a)], once the repulsive interaction U increases, the energy spectra are gapped for periodic boundary due to the weak nonreciprocal hopping, as shown in Figs. S2(c,e) and Fig. S3(b). When the system is changed from the periodic boundary condition to the open one, the lower energy part and the higher energy one cross at $\phi = 2\pi/3$ in the bulk gap regime, and the gapless neutral excitations emerge, as shown in Figs. S2(d,f).

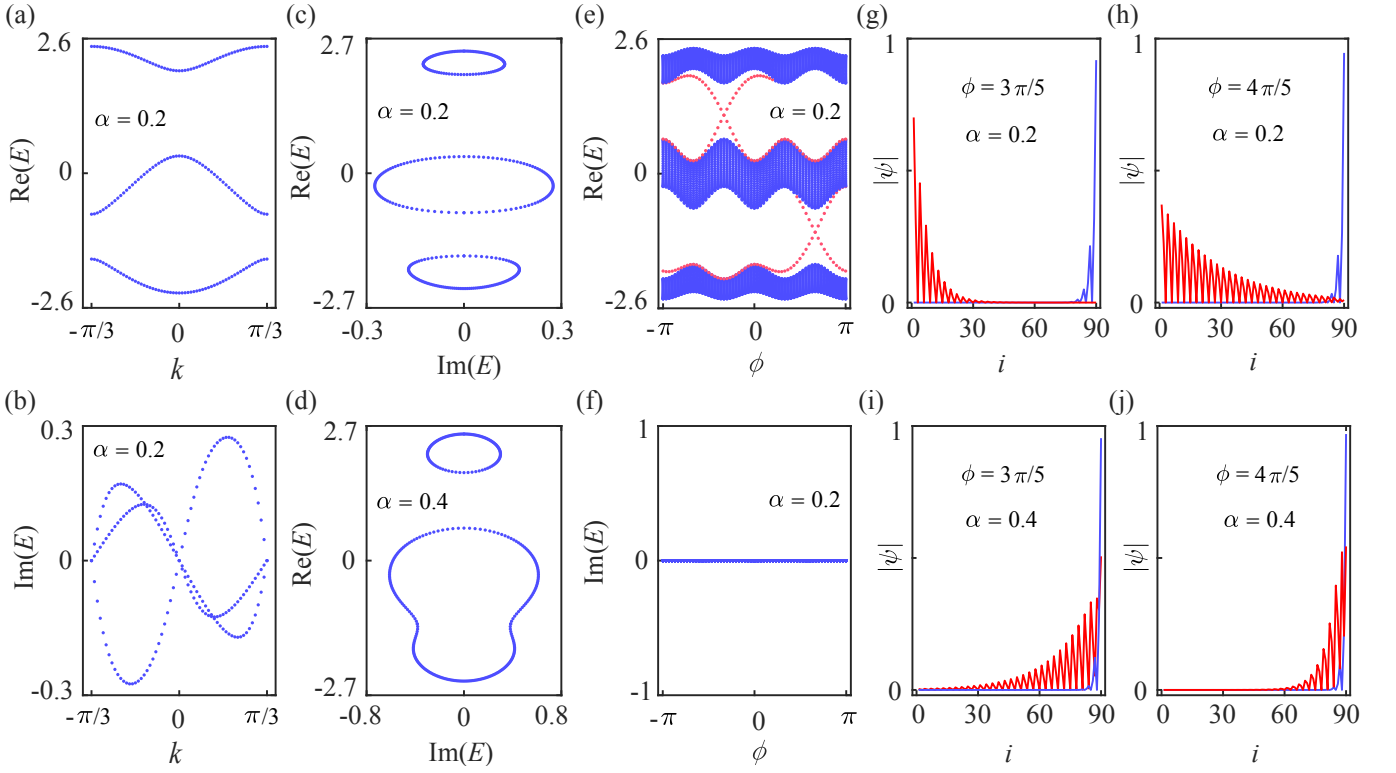


FIG. S1. Non-Hermitian single-particle spectra. (a) Real part and (b) imaginary parts of complex eigenenergies for $\alpha = 0.2$ using the periodic boundary. Real part vs. imaginary part of complex eigenenergies (c) for $\alpha = 0.2$ and (d) for $\alpha = 0.4$ considering the periodic boundary. (e) Real part and (f) imaginary parts of complex eigenenergies as a function of the modulation phase ϕ for $\alpha = 0.2$ using the open boundaries. Red dotted curves indicate the edge modes. (g-j) Spatial density distributions of two mid-gap states at a specific modulation phase ϕ and nonreciprocal hopping factor α . The parameters used here are: $L = 90$, $t = 1$, $V_0 = 1.5$, and $q = 3$.

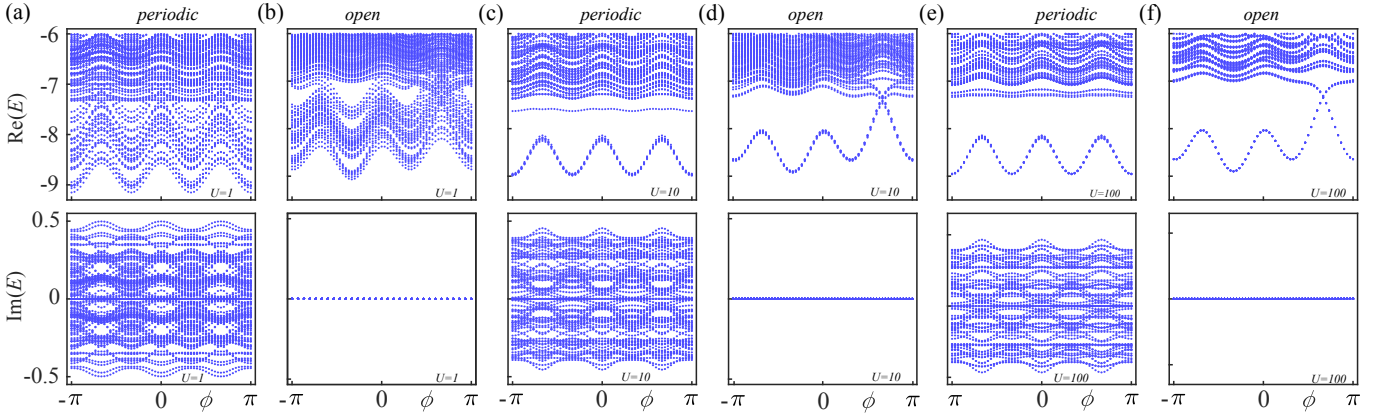


FIG. S2. Low-energy spectra versus the modulation phase ϕ for: (a,b) $U = 1$; (c,d) $U = 10$; and (e,f) $U = 100$. The spectra of (a,c,e) are for periodic boundary, and (b,d,f) for open boundaries. The parameters used here are: $L = 12$, $N_\uparrow = 2$, $N_\downarrow = 2$, $t = 1$, $V_0 = 1.5$, $q = 3$, and $\alpha = 0.2$.

B. Edge excitations of the neutral and charge excitation modes for $U = 10$

In the main text, we discuss the edge excitations of the neutral and charge excitation modes for the strong interaction limit $U = 100$. In this strong interaction limit (in this case, the charge gap is saturated), the interacting system with the nonreciprocal hopping shows the anomalous boundary effect, where some in-gap states exhibit no edge excitations in the open chain. Here we present the results of the edge excitations of the neutral and charge excitation modes for

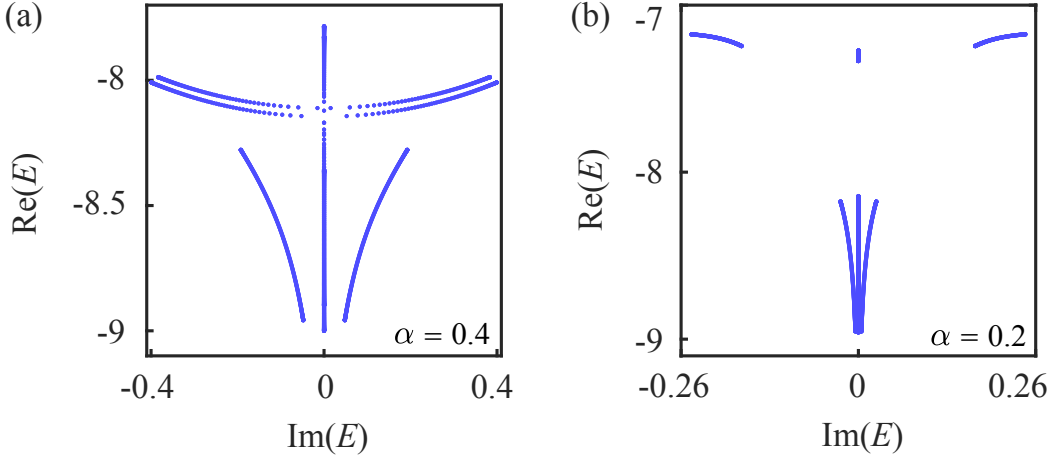


FIG. S3. Few lowest eigenenergies in the complex plane using periodic boundary, for (a) $\alpha = 0.4$, and (b) $\alpha = 0.2$. The parameters used here are: $L = 12$, $N_\uparrow = 2$, $N_\downarrow = 2$, $t = 1$, $V_0 = 1.5$, $q = 3$, and $U = 100$.

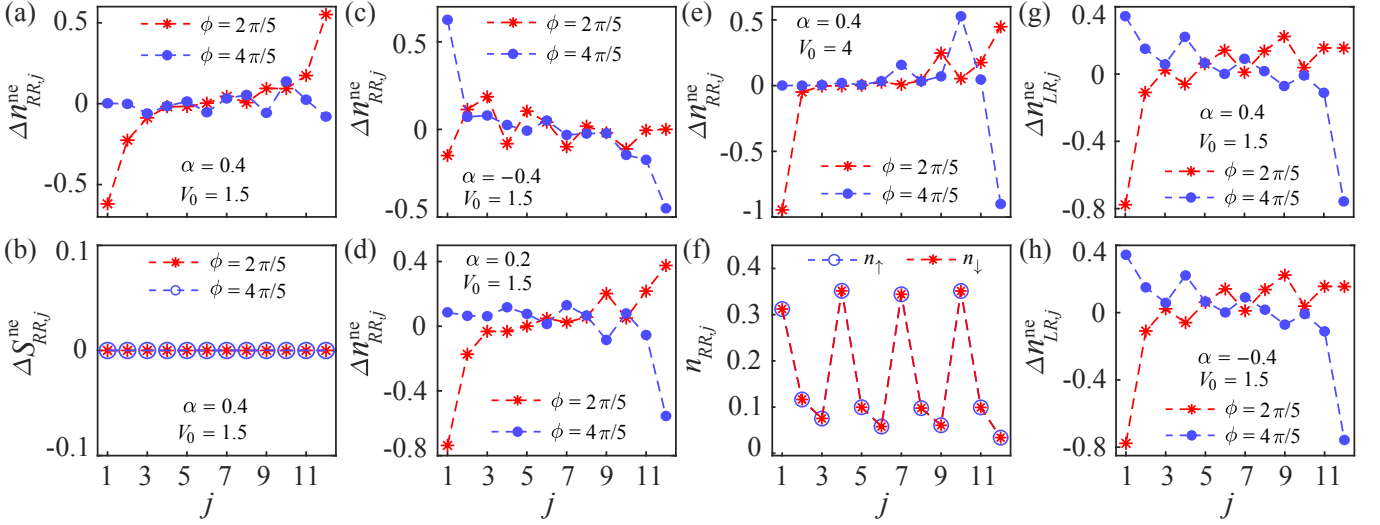


FIG. S4. Spatial distributions of the (a,c,d,e) charge and (b) spin for the neutral excitation modes, calculated via only the right eigenvectors, for different modulation phases ϕ . The spatial distributions are calculated for: (a,b) $\alpha = 0.4$, $V_0 = 1.5$; (c) $\alpha = -0.4$, $V_0 = 1.5$; (d) $\alpha = 0.2$, $V_0 = 1.5$; and (e) $\alpha = 0.4$, $V_0 = 4$. (f) Spin-resolved charge densities of the ground state for $\phi = 2\pi/5$, $\alpha = 0.4$ and $V_0 = 1.5$. The spatial charge distributions calculated via biorthogonal eigenvectors for: (g) $\alpha = 0.4$, $V_0 = 1.5$; and (h) $\alpha = -0.4$; $V_0 = 1.5$. The parameters used here are: $L = 12$, $N_\uparrow = 2$, $N_\downarrow = 2$, $t = 1$, $q = 3$, $V_0 = 1.5$, and $U = 10$.

the weaker interaction $U = 10$ considering the open boundary conditions, as shown in Figs. S4 and S5. As the same as the case for $U = 100$, the neutral and charge excitations, calculated by only the right eigenvectors, also show the same anomalous boundary effect in the weaker interaction. The edge excitations of in-gap states can be correctly characterized only by biorthogonal eigenvectors.

C. Spatial charge density distributions

In this part, we present the charge density distributions, and demonstrate that the anomalous boundary effect results from the combined effects of the nonreciprocal hopping, superlattice modulation, and interactions. Figure S6 plots the spin-resolved charge densities, calculated by only the right eigenvectors, of the higher-excited state $|\Phi_1(N_\uparrow, N_\downarrow)\rangle_R$ (the first row) and the ground state $|\Phi_0(N_\uparrow, N_\downarrow)\rangle_R$ (the second row) for $\alpha = 0.4$ and $\alpha = 0$. Their

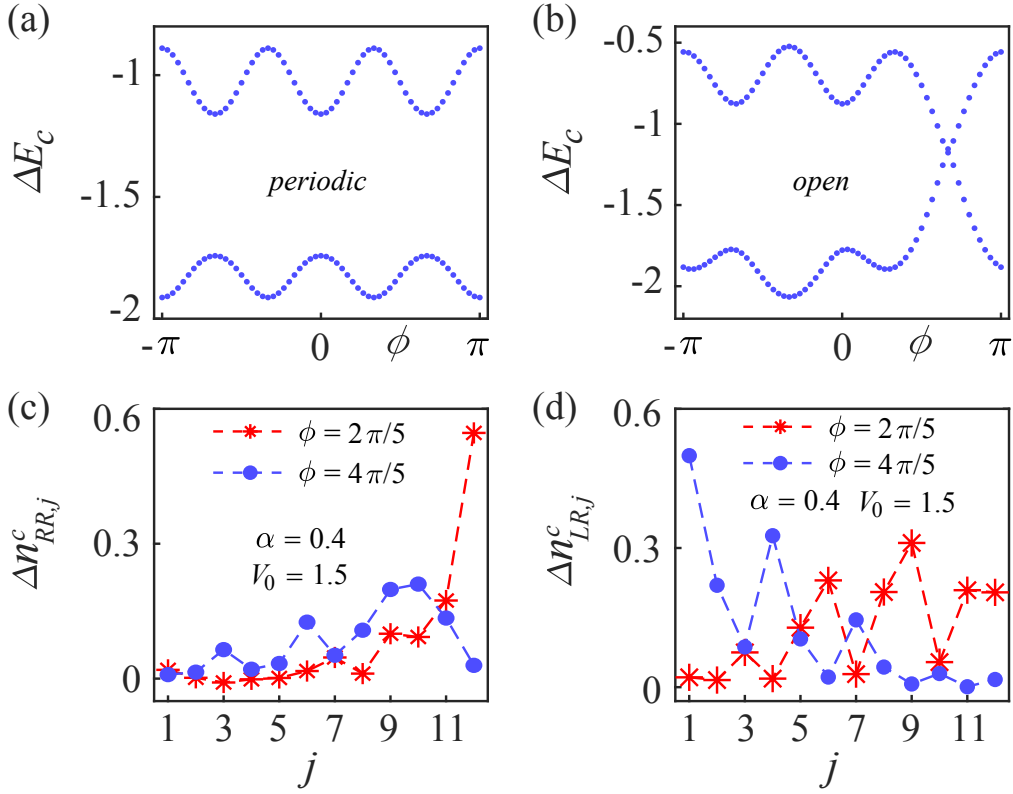


FIG. S5. Charge excitation spectra $\Delta E_c(2,2)$ and $\Delta E_c(2,1)$ versus the modulation phase ϕ for (a) periodic and (b) open boundaries. The spatial charge distributions, calculated using (c) only the right eigenvectors and (d) biorthogonal eigenvectors, of the charge excitations for different modulation phases ϕ . The parameters used here are: $L = 12$, $N_\uparrow = 2$, $N_\downarrow = 2$, $t = 1$, $q = 3$, $V_0 = 1.5$, and $U = 10$.

difference defines the corresponding charge distributions of the neutral excitations [see Eq. (2) in the main text]. The black dotted line indicates the superlattice potential $V_j = V_0 \cos(2\pi j/q + \phi)$ for $\phi = 2\pi/5$ and $\phi = 4\pi/5$.

For the Hermitian case with $\alpha = 0$, due to the spatial modulations of the superlattice potential, the charge densities in the bulk exhibit periodic oscillations, and the neutral excitations are localized at the ends, for both $\phi = 2\pi/5$ and $\phi = 4\pi/5$, as indicated in Figs. S6(c,d).

For the non-Hermitian case with $\alpha = 0.4$, the charge densities are also periodically modulated by the superlattice potential. The particles in the bulk do not accumulate towards the right end, in spite of the stronger forward-hopping amplitude, due to the Pauli exclusion principle and on-site interactions. In order to minimize the energy in the ground state $|\Phi_0(N_\uparrow, N_\downarrow)\rangle_R$ (the second row), the site where the superlattice potential V_j is lower is occupied by more charges. As shown in Figs. S6(a,c) and Figs. S6(b,d), to minimize the ground-state energy, the left end is occupied by more particles than the right end for $\phi = 2\pi/5$; while the right end is occupied by more particles than the left end for $\phi = 4\pi/5$. In the excited state $|\Phi_1(N_\uparrow, N_\downarrow)\rangle_R$ (the first row), the nonreciprocal hopping somehow pushes the particles towards the right end both for $\phi = 2\pi/5$ and $\phi = 4\pi/5$ [Figs. S6(a,b)]. As a result, the neutral excitation is still localized at the ends for $\phi = 2\pi/5$ and $\alpha = 0.4$, but the edge neutral excitations disappear for $\phi = 4\pi/5$ and $\alpha = 0.4$.

Moreover, when the modulation potential increases from the $V_0 = 1.5$ to $V_0 = 4$ [see Fig. 3(e) in the main text], the nonreciprocal hopping is weakened by the potential barrier for the higher-energy states; therefore, the neutral excitation is localized at ends for $\phi = 4\pi/5$ and $V_0 = 4$. In conclusion, the anomalous boundary effect of the neutral excitation results from the combined effects of nonreciprocal hopping, superlattice modulation, and interactions.

The anomalous boundary effect occurring for the charge excitations can also be explained in a similar way. Figure S7 plots the charge densities of the ground state $|\Phi_0(N_\uparrow, N_\downarrow)\rangle_R$ (the first row) and $|\Phi_0(N_\uparrow, N_\downarrow + 1)\rangle_R$ (the second row). Their difference defines the corresponding charge distributions of the charge excitations [see Eq. (5) in the main text]. Due to the spatial modulations of the superlattice potential, the charge densities in the bulk exhibit periodic oscillations. To minimize the system energy in the ground state, the site where the superlattice potential V_j is lower is occupied by more charges. Therefore, in the ground state $|\Phi_0(N_\uparrow, N_\downarrow)\rangle_R$ (the first row), the left end is occupied

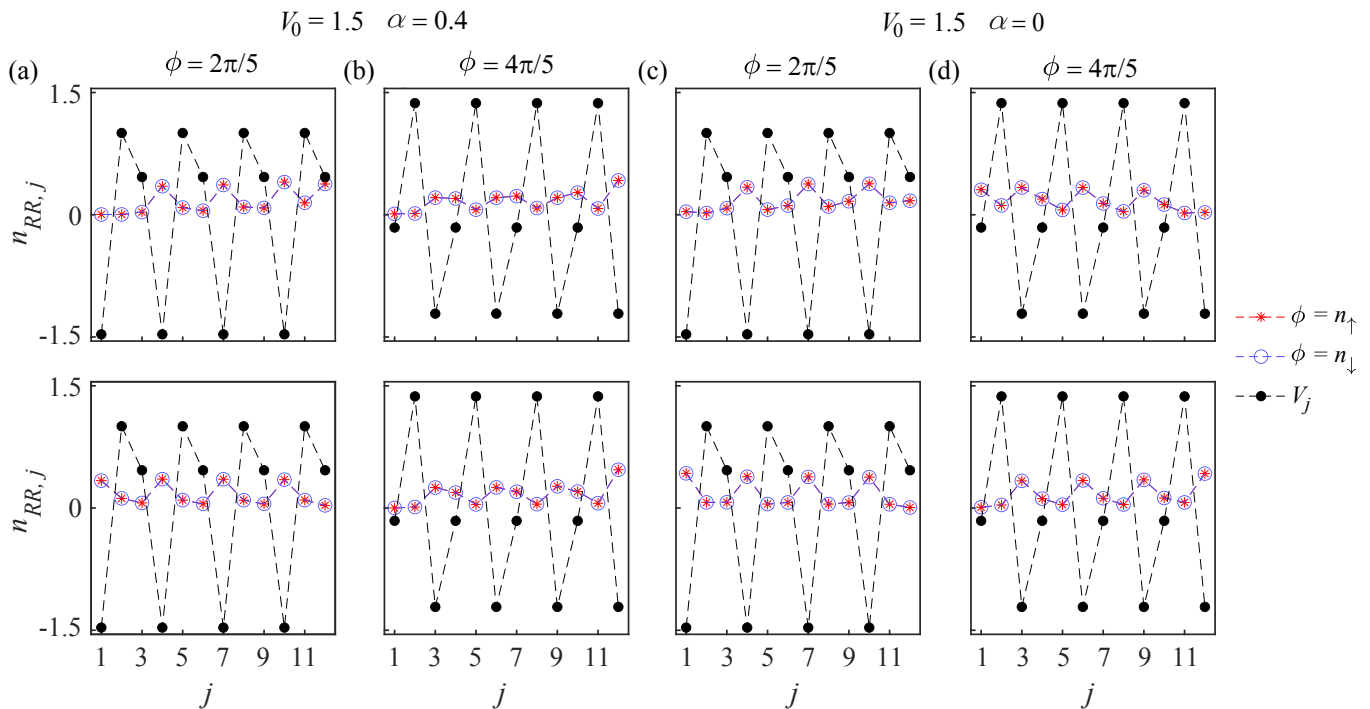


FIG. S6. Spin-resolved charge densities, calculated via only the right eigenvectors, of the ground state $|\Phi_0(N_\uparrow, N_\downarrow)\rangle_R$ (the second row) and the higher energy state $|\Phi_1(N_\uparrow, N_\downarrow)\rangle_R$ (the first row) for (a,b) $\alpha = 0.4$, and (c,d) $\alpha = 0$ using the open boundaries. The black dotted line indicates the superlattice potential $V_j = V_0 \cos(2\pi j/q + \phi)$. The parameters used here are: $L = 12$, $N_\uparrow = 2$, $N_\downarrow = 2$, $t = 1$, $q = 3$, $V_0 = 1.5$, and $U = 100$.

by more particles than the right end for $\phi = 2\pi/5$, while the right end is occupied by more particles than the left end for $\phi = 4\pi/5$. When an extra particle is added, in the ground state $|\Phi_0(N_\uparrow, N_\downarrow + 1)\rangle_R$ (the second row), it tends to occupy the right end for $\alpha = 0.4$ due to the stronger forward hopping. This leads to the absence of the charge excitations for $\phi = 4\pi/5$ and $\alpha = 0.4$.

D. Neutral and charge excitation spectra for $v_\uparrow = 1/5$ and $v_\downarrow = 4/5$

For the considered non-Hermitian model in the presence of the superlattice potential, as long as the total filling factor $v = \sum_{\sigma=\uparrow,\downarrow} v_\sigma = \sum_{\sigma=\uparrow,\downarrow} N_\sigma/N_{\text{cell}} = 1$, the interaction can drive the metallic phase into the topological Mott insulator, which shows the anomalous boundary effect in the presence of the nonreciprocal hopping. To demonstrate this, here we present the results of neutral and charge excitation spectra for filling factors $v_\uparrow = 1/5$ and $v_\downarrow = 4/5$ with $L = 15$, as shown in Figs. S8-S12. The results show there exist both gapless neutral and charge excitations localized at the edges. The interplay of nonreciprocal hopping, superlattice potential, and strong correlations leads to the absence of edge excitations, defined by only the right eigenvectors, of some in-gap modes appearing in both the neutral and charge excitation spectra. Moreover, these edge excitations can be characterized by using biorthogonal eigenvectors.

E. Possible experimental realization

To realize the non-Hermitian Fermi-Hubbard model with asymmetric hopping in the ultracold atom systems, we can employ reservoir engineering [S2]. We rewrite the system Hamiltonian Eq. (1) in the main text into Hermitian

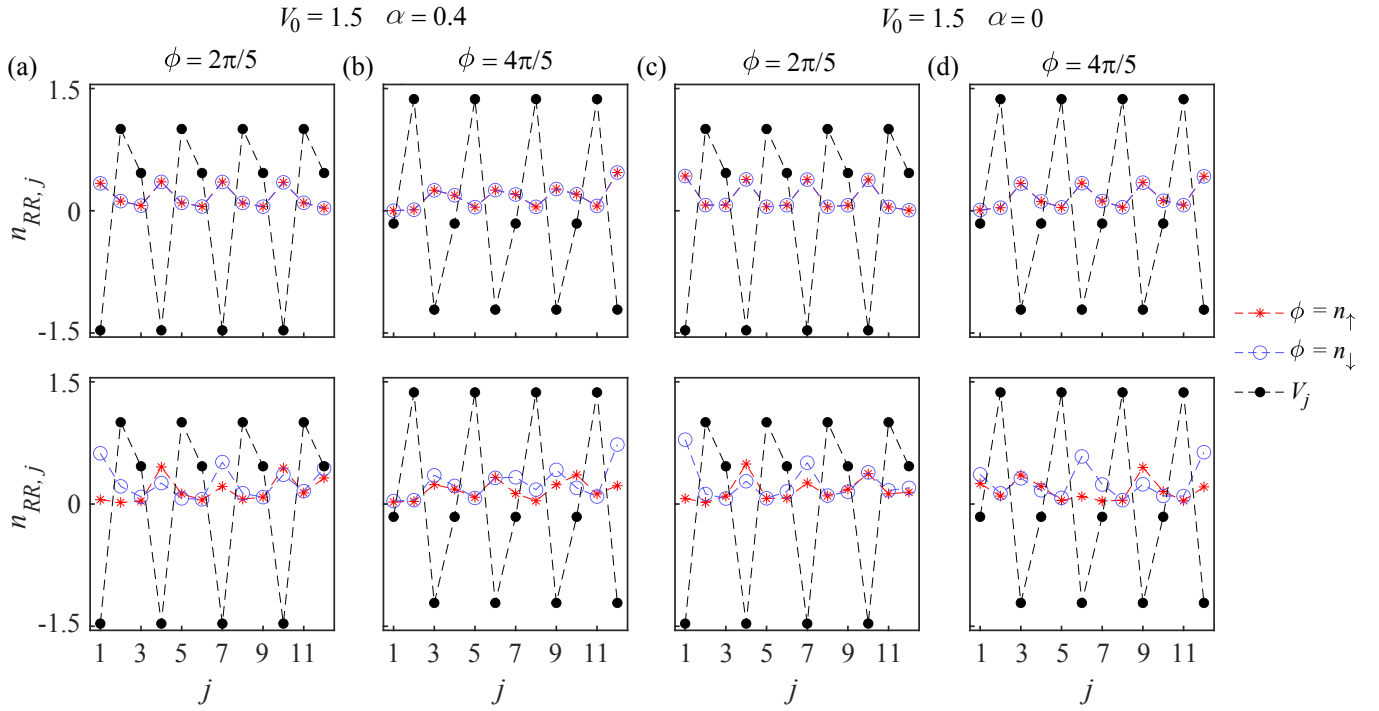


FIG. S7. Spin-resolved charge densities, calculated via only the right eigenvectors, of the ground states $|\Phi_0(N_\uparrow, N_\downarrow)\rangle_R$ (the first row) and $|\Phi_0(N_\uparrow, N_\downarrow + 1)\rangle_R$ (the second row) for (a,b) $\alpha = 0.4$, and (c,d) $\alpha = 0$ using the open boundaries. The black dotted line indicates the superlattice potential $V_j = V_0 \cos(2\pi j/q + \phi)$. The parameters used here are: $L = 12$, $N_\uparrow = 2$, $N_\downarrow = 2$, $t = 1$, $q = 3$, $V_0 = 1.5$, and $U = 100$.

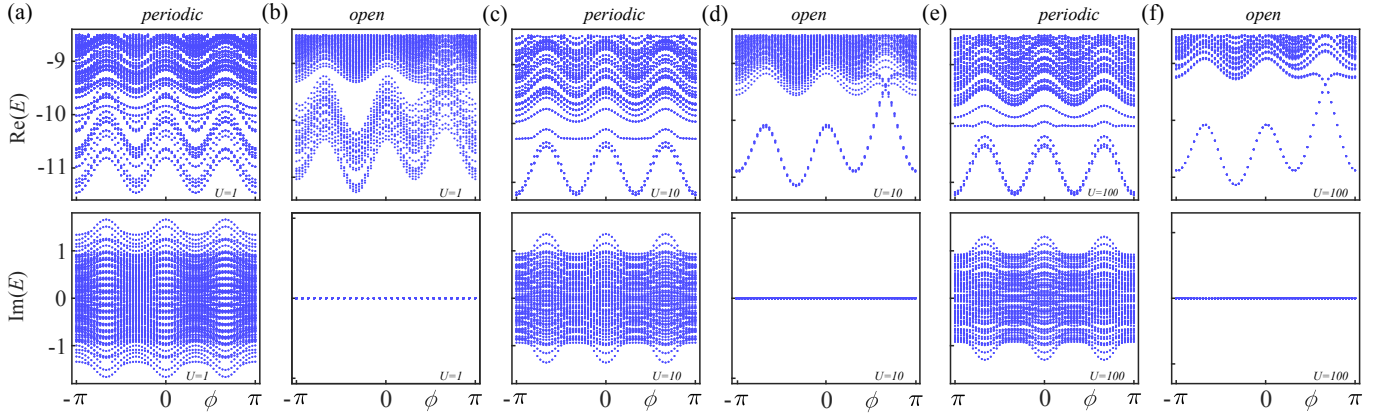


FIG. S8. Low-energy spectra versus the modulation phase ϕ for: (a,b) $U = 1$; (c,d) $U = 10$; and (e,f) $U = 100$. The spectra of (a,c,e) are for periodic boundary, and (b,d,f) for open boundaries. The parameters used here are: $L = 15$, $N_\uparrow = 1$, $N_\downarrow = 4$, $t = 1$, $V_0 = 1.5$, $q = 3$, and $\alpha = 0.4$.

\mathcal{H}_1 and anti-Hermitian \mathcal{H}_2 parts:

$$\mathcal{H}_1 = \frac{1}{2} (\mathcal{H} + \mathcal{H}^\dagger) = -\frac{t(e^\alpha + e^{-\alpha})}{2} \sum_{j,\sigma} (c_{j+1,\sigma}^\dagger c_{j,\sigma} + c_{j,\sigma}^\dagger c_{j+1,\sigma}) + \sum_{j,\sigma} V_j n_{j,\sigma} + U \sum_j c_{j,\uparrow}^\dagger c_{j,\downarrow}^\dagger c_{j,\downarrow} c_{j,\uparrow}, \quad (\text{S4})$$

$$\mathcal{H}_2 = \frac{1}{2} (\mathcal{H} - \mathcal{H}^\dagger) = -\frac{t(e^\alpha - e^{-\alpha})}{2} \sum_{j,\sigma} (c_{j+1,\sigma}^\dagger c_{j,\sigma} - c_{j,\sigma}^\dagger c_{j+1,\sigma}), \quad (\text{S5})$$

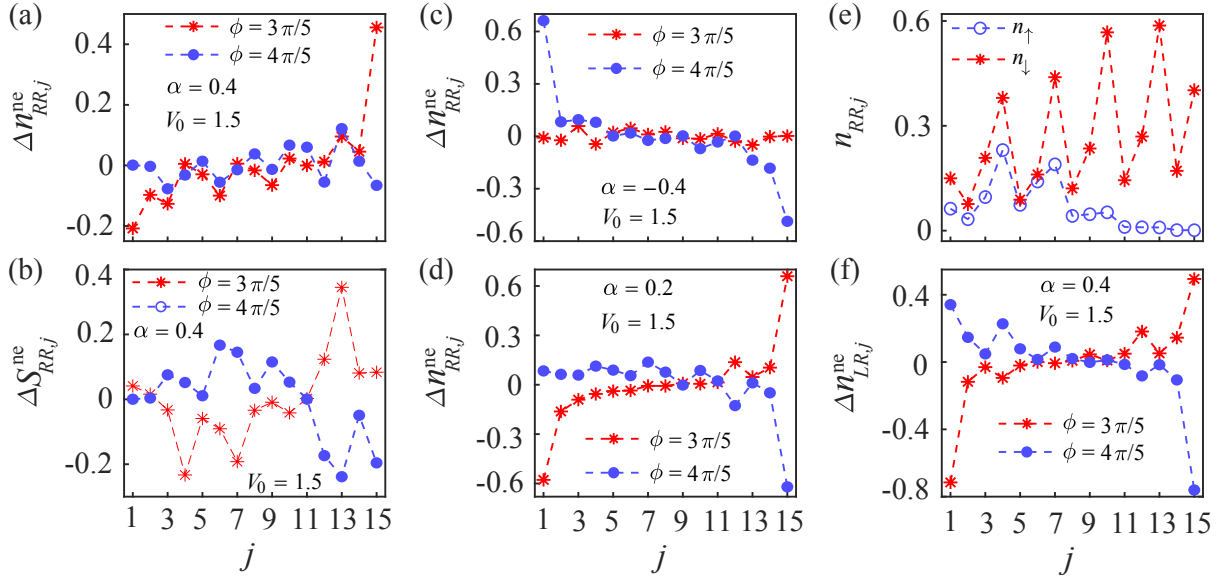


FIG. S9. Spatial distributions of the (a,c,d) charge and (b) spin for the neutral excitation modes, calculated via only the right eigenvectors, for different modulation phases ϕ . Spatial distributions are calculated for: (a,b) $\alpha = 0.4$; (c) $\alpha = -0.4$; and (d) $\alpha = 0.2$. (e) The spin-resolved charge densities of the ground state for $\phi = 3\pi/5$ and $\alpha = 0.4$. (f) Spatial charge distributions calculated via biorthogonal eigenvectors for $\alpha = 0.4$. The parameters used here are: $L = 15$, $N_{\uparrow} = 1$, $N_{\downarrow} = 4$, $t = 1$, $q = 3$, $V_0 = 1.5$, and $U = 10$.

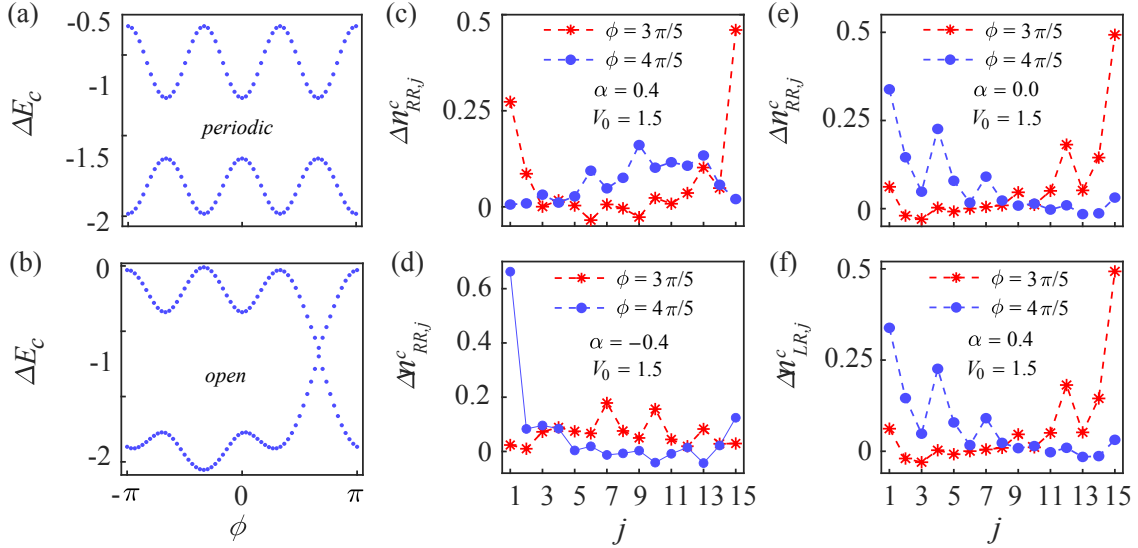


FIG. S10. Charge excitation spectra $\Delta E_c(1,4)$ and $\Delta E_c(1,3)$ versus the modulation phase ϕ for (a) periodic and (b) open boundaries. (c) Spatial charge distributions, calculated using only the right eigenvectors, of the charge excitations for different modulation phases ϕ for: $\alpha = 0.4$; (d) $\alpha = -0.4$; and (e) $\alpha = 0$. (f) Spatial charge distributions, calculated using biorthogonal eigenvectors with $\alpha = 0.4$. The parameters used here are: $L = 15$, $N_{\uparrow} = 1$, $N_{\downarrow} = 4$, $t = 1$, $q = 3$, $V_0 = 1.5$, and $U = 10$.

To engineer this anti-Hermitian part \mathcal{H}_2 , we follow the method developed in Ref. [S2] to dissipatively engineer the following jump operators that describe the collective loss of two nearest-neighbor sites:

$$L_j = \sqrt{t(e^\alpha - e^{-\alpha}) \text{sgn}(\alpha)} [c_{j,\sigma} + i \text{sgn}(\alpha) c_{j+1,\sigma}], \quad (\text{S6})$$

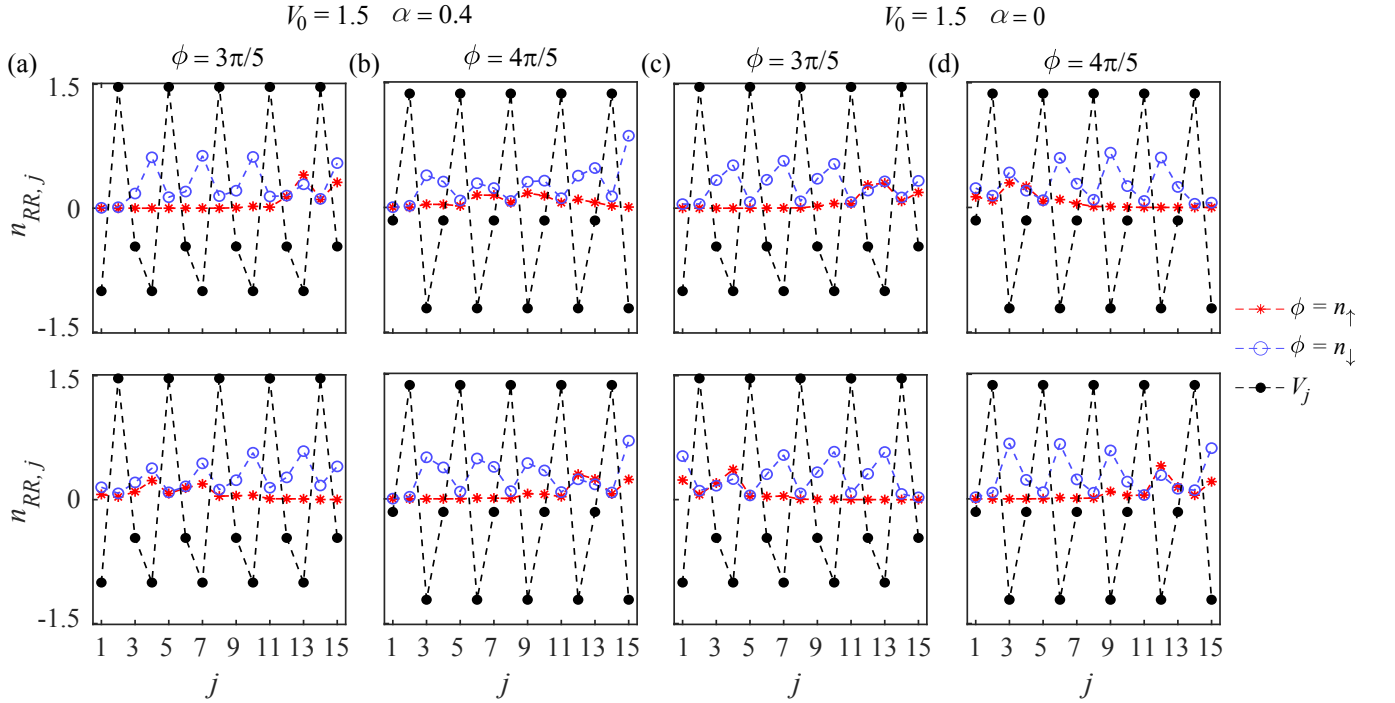


FIG. S11. Spin-resolved charge densities, calculated via only the right eigenvectors, of the ground state $|\Phi_0(N_\uparrow, N_\downarrow)\rangle_R$ (the second row) and the higher energy state $|\Phi_1(N_\uparrow, N_\downarrow)\rangle_R$ (the first row) for (a,b) $\alpha = 0.4$, and (c,d) $\alpha = 0$ using the open boundaries. The black dotted line indicates the superlattice potential $V_j = V_0 \cos(2\pi j/q + \phi)$. The parameters used here are: $L = 15$, $N_\uparrow = 1$, $N_\downarrow = 4$, $t = 1$, $q = 3$, $V_0 = 1.5$, and $U = 10$.

where sgn refers to \pm signs. Then, the open quantum system dynamics with post-selection measurements is determined by the non-Hermitian effective Hamiltonian:

$$H_{\text{eff}} = \mathcal{H} - \frac{i}{2} \sum_j L_j^\dagger L_j = \mathcal{H} - i \frac{t(e^\alpha - e^{-\alpha}) \text{sgn}(\alpha)}{2} \sum_j c_{j,\sigma}^\dagger c_{j,\sigma}, \quad (\text{S7})$$

which differs from the Hamiltonian Eq. (1) in the main text only by a background loss term.

The Hermitian part \mathcal{H}_1 in Eq. (S4) with the superlattice structure can be constructed by loading the ultracold fermionic atoms in the lowest band of a bichromatic optical lattice [S3–S8], and such a Hamiltonian has been experimentally realized [S8]. The bichromatic potential resulting from the superposition of two lattices [a main optical lattice $V_1(x)$ and a secondary weak one $V_2(x)$] can be written as [S3–S5]:

$$V(x) = V_1(x) + V_2(x) = V_1 \cos^2(k_1 x) + V_2 \cos^2(k_2 x + \phi), \quad (\text{S8})$$

where $k_i = 2\pi/\lambda_i$ ($i = 1, 2$) are the lattice wavenumbers, λ_i the wavelength of the lasers which are utilized to form the optical lattices, and V_i are the depth of the lattices with $V_1 \gg V_2$. The period of the superlattice potential $V(x)$ is determined by the ratio $q = k_1/k_2$.

In the strong potential V_1 limit, which is much larger than the recoil energy $E_r = \hbar k_1^2/2M$ with the atomic mass M [S3–S5], we can only consider the lowest Bloch band. Then, the ultracold fermionic atoms in the bichromatic lattices, in the tight-binding limit, can be mapped onto the Hamiltonian \mathcal{H}_1 in Eq. (S4).

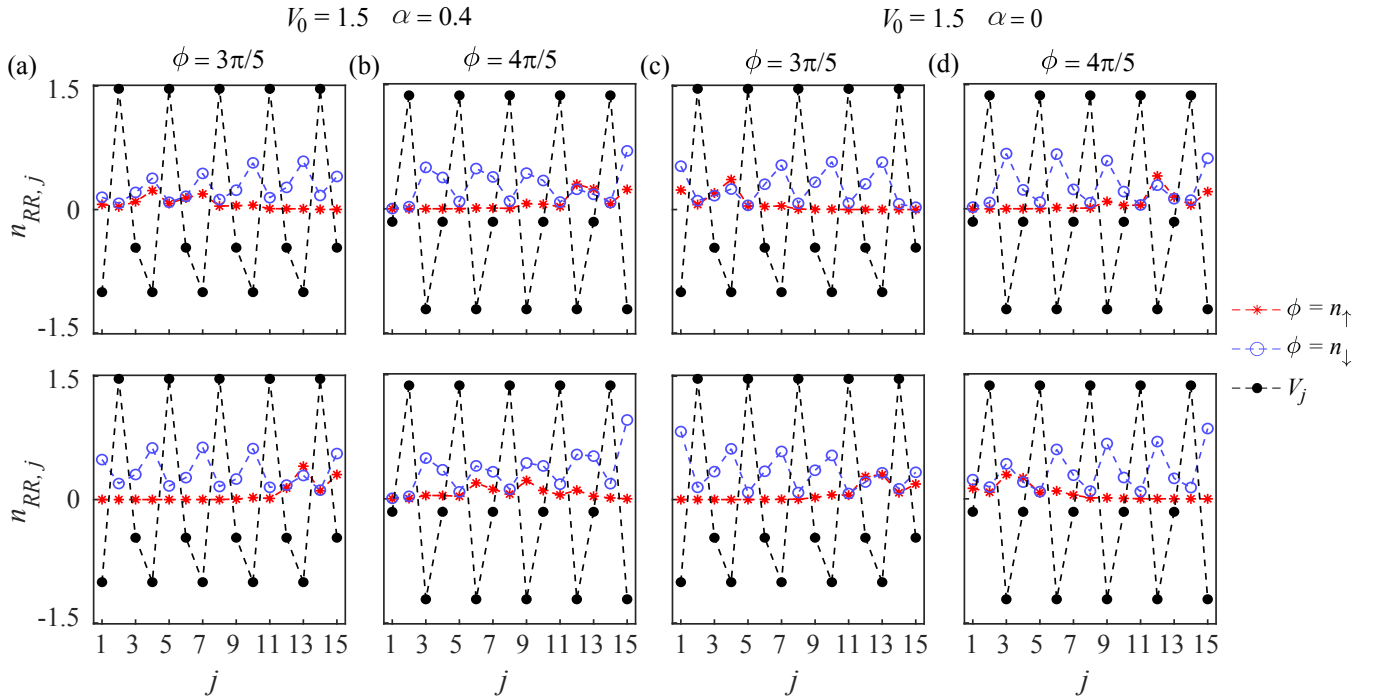


FIG. S12. Spin-resolved charge densities, calculated via only the right eigenvectors, of the ground states $|\Phi_0(N_\uparrow, N_\downarrow)\rangle_R$ (the first row) and $|\Phi_0(N_\uparrow, N_\downarrow + 1)\rangle_R$ (the second row) for (a,b) $\alpha = 0.4$, and (c,d) $\alpha = 0$ using the open boundaries. The black dotted line indicates the superlattice potential $V_j = V_0 \cos(2\pi j/q + \phi)$. The parameters used here are: $L = 15$, $N_\uparrow = 1$, $N_\downarrow = 4$, $t = 1$, $q = 3$, $V_0 = 1.5$, and $U = 10$.

III. Non-Hermitian model with complex-valued interaction

A. Effective Hamiltonian

We now discuss the strongly correlated topological phases with complex-valued interactions. We consider 1D spin-1/2 ultracold fermionic atoms loaded in a bichromatic optical lattice, described by $\mathcal{H} = \mathcal{H}_0 + \mathcal{H}_{\text{int}}$ with

$$\mathcal{H}_0 = -t \sum_{j,\sigma} \left(c_{j,\sigma}^\dagger c_{j+1,\sigma} + c_{j+1,\sigma}^\dagger c_{j,\sigma} \right) + \sum_{j,\sigma} V_j n_{j,\sigma}, \quad (\text{S9})$$

$$\mathcal{H}_{\text{int}} = U \sum_j c_{j,\uparrow}^\dagger c_{j,\downarrow}^\dagger c_{j,\downarrow} c_{j,\uparrow}, \quad (\text{S10})$$

where $V_j = V_0 \cos(2\pi\beta j + \phi)$ denotes a commensurate superlattice potential with modulation frequency $\beta = 1/3$ and phase ϕ , $c_{j,\sigma}^\dagger$ is the fermionic creation operator with spin σ , $n_{j,\sigma} = c_{j,\sigma}^\dagger c_{j,\sigma}$ is the on-site particle number operator, and U denotes the on-site interaction strength. Now we consider two-body inelastic collisions between ultracold atoms, which leads to losses of atoms [S9]. The dissipative dynamics of the system is described by the following quantum master equation [S10]

$$\begin{aligned} \frac{d\rho}{dt} &= -i[\mathcal{H}, \rho] - \frac{\gamma}{2} \sum_j \left(L_j^\dagger L_j \rho + \rho L_j^\dagger L_j - 2L_j \rho L_j^\dagger \right) \\ &= -i[\mathcal{H}_{\text{eff}}, \rho] + \gamma \sum_j L_j \rho L_j^\dagger, \end{aligned} \quad (\text{S11})$$

where ρ is the density matrix of the ultracold atoms, and the Lindblad operator $L_j = c_{j,\downarrow} c_{j,\uparrow}$ describes a two-particle loss at site j with rate γ . According to the quantum-trajectory theory [S11-S13], the dynamics of the dissipative quantum system described by the first line in Eq. (S11) can be decomposed into two processes: a non-unitary

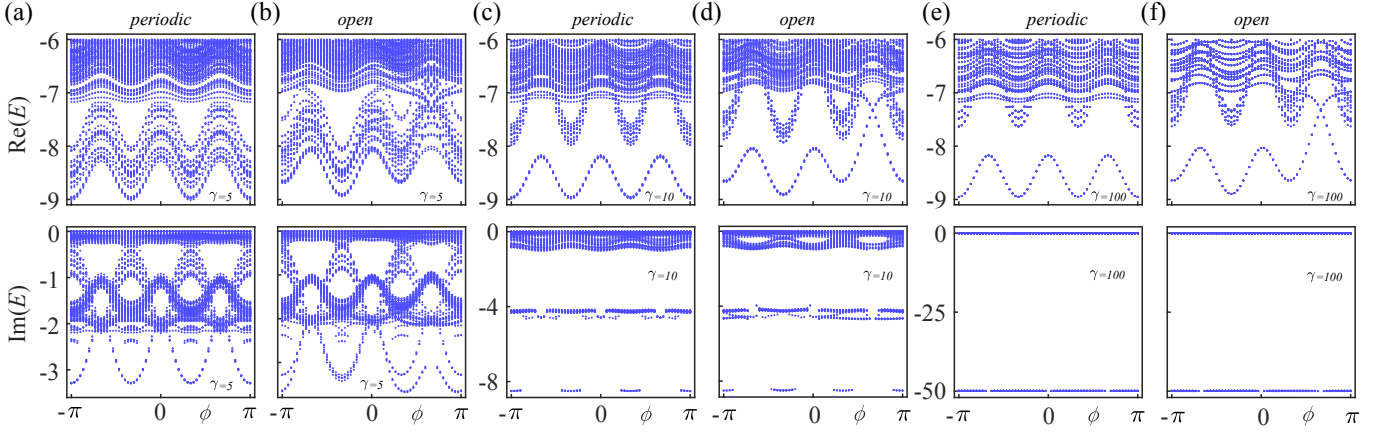


FIG. S13. Low-energy spectrum versus the modulation phase ϕ for: (a,b) $\gamma = 5$; (c,d) $\gamma = 10$; and (e,f) $\gamma = 100$. The spectra in (a,c,e) are for periodic boundary, and in (b,d,f) using open boundaries. The parameters used here are: $L = 12$, $N_{\uparrow} = 2$, $N_{\downarrow} = 2$, $t = 1$, $V_0 = 1.5$, $q = 3$, and $U = 0$.

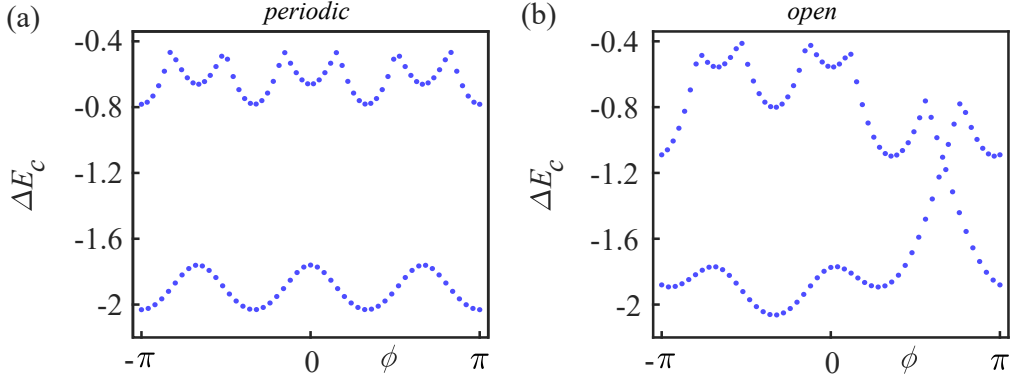


FIG. S14. Charge excitation spectra $\Delta E_c(2,2)$ and $\Delta E_c(2,1)$ versus the modulation phase ϕ for (a) periodic and (b) open boundaries. The parameters used here are: $\gamma = 100$, $L = 12$, $N_{\uparrow} = 2$, $N_{\downarrow} = 2$, $t = 1$, $V_0 = 1.5$, $q = 3$, and $U = 0$.

Schrödinger evolution described by the effective non-Hermitian Hamiltonian $\mathcal{H}_{\text{eff}} = \mathcal{H} - i\gamma/2 \sum_j L_j^\dagger L_j$, and stochastic quantum jumps, described by the second term in the second line of Eq. (S11), which leads to atomic losses. Therefore, when projecting out the quantum jumps (by continuously monitoring the particle number [S14, S15]), the system is governed by the following effective non-Hermitian Hamiltonian with a complex-valued on-site interaction

$$\mathcal{H}_{\text{eff}} = \mathcal{H}_0 + (U - i\gamma/2) \sum_j c_{j,\uparrow}^\dagger c_{j,\downarrow}^\dagger c_{j,\downarrow} c_{j,\uparrow}. \quad (\text{S12})$$

B. Low-energy spectra of neutral and charge excitations

Figures S13 and S14 show the low-energy spectra of neutral and charge excitations for the purely imaginary-valued interactions using both periodic and open boundary conditions, respectively. According to the neutral excitation spectra, for a small absolute value of the interaction strength, e.g., $\gamma = 5$, there exist no gaps using both periodic [Fig. S13(a)] and open [Fig. S13(b)] boundary conditions. However, for large absolute values of the interaction strengths, e.g., $\gamma = 10$ and $\gamma = 100$, the energy gaps are opened for periodic boundary condition, as shown in Figs. S13(c) and S13(e). The gap opening indicates that the purely imaginary-valued on-site interaction here plays the roles of the effective repulsion between the two-component fermions, which can be attributed to the continuous quantum Zeno effect [S9, S16–S18]. When the system goes from periodic to open boundaries, the in-gap modes, which connect the lower-energy and higher-excited sectors, appear. The gapless modes here closely resemble the appearance of edge states in the single-particle spectrum. In contrast to the nonreciprocal case, the many-body spectrum is

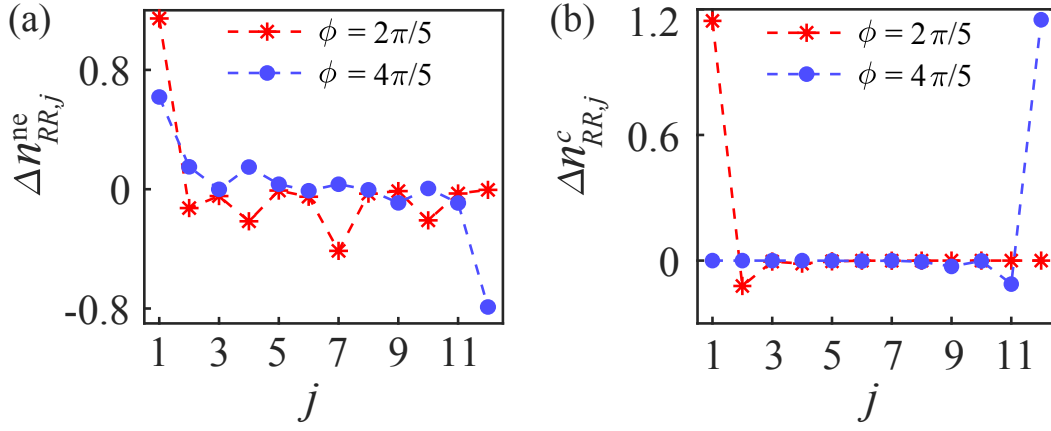


FIG. S15. Spatial charge distributions for the (a) neutral excitation and (b) charge excitation modes for different modulation phases ϕ . The parameters used here are: $\gamma = 100$, $L = 12$, $N_{\uparrow} = 2$, $N_{\downarrow} = 2$, $t = 1$, $V_0 = 1.5$, $q = 3$, and $U = 0$.

complex. Note that the lower-energy sector become broader for smaller interaction strengths due to spin fluctuations. Furthermore, for the periodic boundary, the charge excitation spectrum is gaped for $\gamma = 100$ [see Fig. S14(a)], and the gapless edge excitations emerge once the boundary is opened [see Fig. S14(b)].

Once the boundary is opened, in-gap modes emerge. The spatial charge distributions for the neutral and charge excitations are plotted in Figs. S15(a,b), where the in-gap modes are well localized at the edges. Note that these exhibit the same spatial distribution calculated by biorthogonal eigenvectors, for the neutral and charge excitations, as the one using only right eigenvectors. No anomalous boundary effect occurs for purely imaginary-valued interactions.

* E-mail: tao.liu@riken.jp

† E-mail: fnori@riken.jp

- [S1] L. J. Lang, X. Cai, and S. Chen, “Edge states and topological phases in one-dimensional optical superlattices,” *Phys. Rev. Lett.* **108**, 220401 (2012).
- [S2] Z. Gong, Y. Ashida, K. Kawabata, K. Takasan, S. Higashikawa, and M. Ueda, “Topological phases of non-Hermitian systems,” *Phys. Rev. X* **8**, 031079 (2018).
- [S3] G. Roux, T. Barthel, I. P. McCulloch, C. Kollath, U. Schollwöck, and T. Giamarchi, “Quasiperiodic Bose-Hubbard model and localization in one-dimensional cold atomic gases,” *Phys. Rev. A* **78**, 023628 (2008).
- [S4] M. Lewenstein, A. Sanpera, and V. Ahufinger, *Ultracold Atoms in Optical Lattices* (Oxford University Press, 2012).
- [S5] H. Hu, S. Chen, T. S. Zeng, and C. Zhang, “Topological Mott insulator with bosonic edge modes in one-dimensional fermionic superlattices,” *Phys. Rev. A* **100**, 023616 (2019).
- [S6] V. Guarrera, L. Fallani, J. E. Lye, C. Fort, and M. Inguscio, “Inhomogeneous broadening of a Mott insulator spectrum,” *New J. Phys.* **9**, 107 (2007).
- [S7] G. Roati, C. D’Errico, L. Fallani, M. Fattori, C. Fort, M. Zaccanti, G. Modugno, M. Modugno, and M. Inguscio, “Anderson localization of a non-interacting Bose–Einstein condensate,” *Nature* **453**, 895 (2008).
- [S8] M. Schreiber, S. S. Hodgman, P. Bordia, H. P. Luschen, M. H. Fischer, R. Vosk, E. Altman, U. Schneider, and I. Bloch, “Observation of many-body localization of interacting fermions in a quasirandom optical lattice,” *Science* **349**, 842 (2015).
- [S9] T. Tomita, S. Nakajima, I. Danshita, Y. Takasu, and Y. Takahashi, “Observation of the Mott insulator to superfluid crossover of a driven-dissipative Bose-Hubbard system,” *Sci. Adv.* **3**, e1701513 (2017).
- [S10] H. P. Breuer and F. Petruccione, *The Theory of Open Quantum Systems* (Oxford University Press, 2007).
- [S11] P. Meystre and M. Sargent, eds., *Elements of Quantum Optics* (Springer Berlin Heidelberg, 2007).
- [S12] J. Dalibard, Y. Castin, and K. Mølmer, “Wave-function approach to dissipative processes in quantum optics,” *Phys. Rev. Lett.* **68**, 580 (1992).
- [S13] H. J. Carmichael, “Quantum trajectory theory for cascaded open systems,” *Phys. Rev. Lett.* **70**, 2273 (1993).
- [S14] Y. Ashida, S. Furukawa, and M. Ueda, “Quantum critical behavior influenced by measurement backaction in ultracold gases,” *Phys. Rev. A* **94**, 053615 (2016).
- [S15] Y. Ashida, S. Furukawa, and M. Ueda, “Parity-time-symmetric quantum critical phenomena,” *Nat. Commun.* **8**, 15791 (2017).
- [S16] N. Syassen, D. M. Bauer, M. Lettner, T. Volz, D. Dietze, J. J. Garcia-Ripoll, J. I. Cirac, G. Rempe, and S. Durr, “Strong dissipation inhibits losses and induces correlations in cold molecular gases,” *Science* **320**, 1329 (2008).
- [S17] G. Barontini, R. Labouvie, F. Stubenrauch, A. Vogler, V. Guarrera, and H. Ott, “Controlling the dynamics of an open

- many-body quantum system with localized dissipation,” *Phys. Rev. Lett.* **110**, 035302 (2013).
- [S18] K. Yamamoto, M. Nakagawa, K. Adachi, K. Takasan, M. Ueda, and N. Kawakami, “Theory of Non-Hermitian fermionic superfluidity with a complex-valued interaction,” *Phys. Rev. Lett.* **123**, 123601 (2019).